

# CASE FILE COPY

## SECOND QUARTERLY REPORT

### STUDY & DETERMINATION OF AN OPTIMUM DESIGN FOR SPACE UTILIZED LITHIUM DOPED SOLAR CELLS

15 January 1970

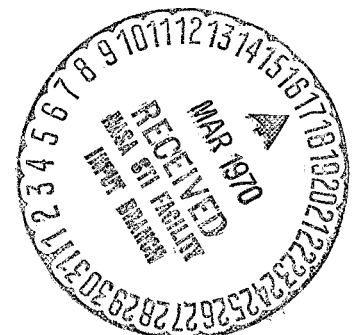
R. G. Downing  
J. R. Carter  
W. K. Van Atta

13154-6006-R0-00

*N70-17299  
CR-107861  
NASA*

Contract 952554

Jet Propulsion Laboratory  
California Institute of Technology  
Pasadena, California



TRW Systems Group  
One Space Park  
Redondo Beach, California 90278

SECOND QUARTERLY REPORT

STUDY & DETERMINATION OF AN OPTIMUM DESIGN FOR  
SPACE UTILIZED LITHIUM DOPED SOLAR CELLS

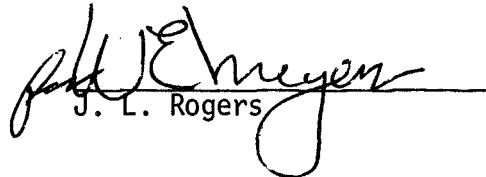
15 January 1970

13154-6006-R0-00

Prepared by:

  
R. G. Downing

Approved by:

  
J. L. Rogers

Contract 952554

Jet Propulsion Laboratory  
California Institute of Technology  
Pasadena, California

TRW Systems Group  
One Space Park  
Redondo Beach, California 90278

This work was performed for the Jet Propulsion Laboratory, California Institute of Technology, as sponsored by the National Aeronautics and Space Administration under Contract 952554.

TABLE OF CONTENTS

	<u>PAGE</u>
ABSTRACT	v
I. KINETICS OF LITHIUM IN SILICON	1
A. Hall Coefficient Measurements	1
B. Carrier Removal Studies in Cells, Quartz-Crucible	3
C. Carrier Removal Studies in Cells, Float-Zone	5
II. LITHIUM SOLAR CELL EVALUATION	8
A. Centralab Cells	9
B. Heliotek Cells	10
C. Texas Instruments Cells	10
D. Summary	10
III. PROGRESS IN THE NEXT REPORT PERIOD	11
IV. NEW TECHNOLOGY	11

LIST OF ILLUSTRATIONS

<u>TABLES</u>		<u>PAGE</u>
I	LITHIUM SOLAR CELL MANUFACTURING PARAMETERS	12
II	LITHIUM SOLAR CELL RECOVERY CHARACTERISTICS	13
III	RECOVERED LEVEL AND HALF RECOVERY TIME (Hours)	14
 <u>FIGURES</u>		
1	HALL COEFFICIENT VS. TEMPERATURE, IRRADIATED LI-DOPED QUARTZ-CRUCIBLE SILICON	15
2	HALL COEFFICIENT VS. TEMPERATURE, IRRADIATED LI-DOPED QUARTZ-CRUCIBLE SILICON	16
3	NORMALIZED HALL COEFFICIENT VS. TEMPERATURE, IRRADIATED LI-DOPED QUARTZ-CRUCIBLE SILICON	17
4	RECOVERY OF LI-DOPED QUARTZ-CRUCIBLE CELL	18
5	DONOR CONCENTRATION VS. BARRIER WIDTH, CELL AF 14-4921	19
6	REMOVAL RATE VS. BARRIER WIDTH, CELL AF 14-4921	20
7	REMOVAL RATE VS. LI CONCENTRATION, CELL AF 14-4921	21
8	SOLAR CELL CHARACTERISTICS, CELL C3-18	22
9	DONOR CONCENTRATION VS. BARRIER, CELL C3-18	23
10	DONOR CONCENTRATION VS. FLUENCE, CELL C3-18	24
11	SOLAR CELL CHARACTERISTICS, CELL Af 14-4903	25
12	DONOR CONCENTRATION VS. BARRIER WIDTH, CELL AF 14-4903	26
13	DONOR CONCENTRATION VS. FLUENCE, CELL AF 14-4903	27
14	SOLAR CELL CHARACTERISTICS, CELL T4-10	28
15	DONOR CONCENTRATION VS. BARRIER WIDTH, CELL T4-10	29
16	REMOVAL RATE VS. LI CONCENTRATION, FLOAT-ZONE CELLS	30
17	REMOVAL RATE VS. BARRIER WIDTH, FLOAT-ZONE CELLS	31
18	RECOVERY OF GROUPS C8A AND C8B LITHIUM SOLAR CELLS	32
19	RECOVERY OF GROUPS C8C AND C8D LITHIUM SOLAR CELLS	33

LIST OF ILLUSTRATIONS (Cont.)

<u>FIGURES</u>		<u>PAGE</u>
20	RECOVERY OF GROUPS C8G AND C8H LITHIUM SOLAR CELLS	34
21	RECOVERY OF GROUP H8 LITHIUM SOLAR CELLS	35
22	RECOVERY OF GROUP T9 LITHIUM SOLAR CELLS	36
23	RECOVERY OF GROUP T10 LITHIUM SOLAR CELLS	37

ABSTRACT

A study of the kinetics of lithium-doped silicon under the influence of electron radiation utilizing Hall coefficient and capacitance measurements on both crucible and float-zone silicon has yielded considerable information. In crucible silicon electron radiation results principally in the formation of silicon A center recombination sites. Subsequent recovery appears to occur by annihilation of the A center through lithium diffusion and interaction. In float-zone silicon, carrier removal rates during irradiation were found to be a strong function of lithium concentration and hence distance from the barrier edge. Removal rates in float-zone silicon during recovery exceed by a significant amount the removal rate during irradiation as contrasted to crucible silicon. The solar cell evaluation of recent groups of lithium-doped solar cells indicate negative results in that the recent groups tested are inferior to the better groups previously tested. Diffusion of oxygen into float-zone silicon and diffusion of lithium from both sides do not appear at this time to enhance the initial and recovery characteristics of lithium-doped cells.

## I. KINETICS OF LITHIUM IN SILICON

During the past quarter considerable progress has been made in experimental studies which indicate the nature of the atomistic model for production and annealing of damage in lithium-doped silicon. This problem was reviewed in our previous quarterly report. The model proposed for float zone silicon appears to be adequate. In the case of quartz-crucible silicon it was obvious that the information needed to formulate a useable model was not available. Our recent work has been directed toward obtaining data to use for this purpose. Separate studies recently completed now appear to support a model for quartz-crucible silicon. In addition, considerable information has been gathered regarding changes in lithium concentration which occur during and after irradiation in lithium-doped float-zone cells.

### A. Hall Coefficient Measurements

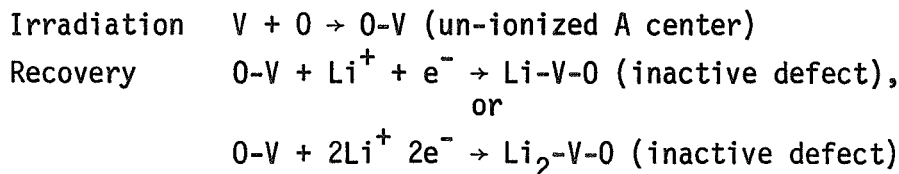
Lithium was diffused into wafers of 50 ohm-cm n-type quartz-crucible silicon to make several Hall specimens. The lithium concentrations were about  $7 \times 10^{14}$  atoms/cm<sup>3</sup>. This doping level is comparable with that found in lithium-doped solar cells. In this way it was hoped that the results would be typical of behavior in lithium-doped solar cells.

Our initial results in the irradiation of this material are shown in Figure 1. The sample was irradiated with a fluence of  $1 \times 10^{16}$  e/cm<sup>2</sup> of 1 MeV electrons. Figure 1 shows a plot of reciprocal Hall coefficient versus reciprocal temperature for sample Q-2A. This reciprocal Hall coefficient can be interpreted as conduction carrier concentration. The before irradiation data indicated a constant electron concentration throughout the temperature range investigated. Irradiation produced a small change in the room temperature electron concentration. The low temperature electron concentration was greatly lowered in a manner that indicates that the irradiation produced a large concentration of acceptor defects with a deep lying level. The manner in which the Hall coefficient of the irradiated specimen changes with temperature indicates that the Fermi level has become pinned to the energy level of the radiation produced defect. The defect energy level calculated from the slope shown in Figure 1 is 0.19 eV below the bottom of the conduction band. This value is not properly corrected

for the temperature variation of the density of states in the conduction band. To properly account for the density of states, the quantity  $\log 1/T^{3/2} R_H$  must be plotted against  $1/T$ . This has the effect of lowering the apparent energy level a small amount. Although this analysis has not been completed, it is apparent that the true energy level will lie very close to the known position of the Si-A center (0.17 eV). This data strongly suggests that one of the main defects produced during room temperature irradiation of lithium-doped quartz-crucible silicon is the Si-A center. A second sample (Q-2C) was irradiated with an electron fluence of  $1 \times 10^{15} \text{ e/cm}^2$ . The data for this sample is shown in Figure 2. It can be seen that there is evidence of a deep level after irradiation and annealing reduces the concentration of deep level defects and conduction electrons. To assist in analysis of the data, it was normalized to the before irradiation results. In this way the temperature variation of the Hall factor is removed from the data. These results are shown in Figure 3. Several observations can be made from this data. The concentration of the deep level defects produced by irradiation is about  $2 \times 10^{14} \text{ cm}^{-2}$ . The indicated defect production rate would be  $0.2 \text{ cm}^{-1}$ . The Si-A center has an energy level at 0.17 eV below conduction band. Assuming a degeneracy factor of 1/2, the two-thirds ionization point will be reached at a temperature of 195°K ( $1000/T^\circ\text{K} = 5.15$ ). Additional calculations show the Fermi level of sample (Q-2C) at 195°K after irradiation to be at 0.17 eV below the bottom of the conduction band. There also appears to be some evidence of other extremely shallow energy level defects, because the carrier concentration is again declining at 120°K. After an anneal of 150 hours at 100°C, the concentration of A centers was reduced to  $7 \times 10^{13} \text{ cm}^{-3}$ . During the same period the concentration of carrier electrons or lithium donors was reduced by  $3.3 \times 10^{14} \text{ cm}^{-3}$ . The loss in A centers was  $1.4 \times 10^{14} \text{ cm}^{-1}$ . These results indicate that roughly 2 lithium donors are consumed in the anneal of 1 Si-A center. This behavior is very similar to that reported by Vavilov (Radiation Damage in Semiconductors, p. 115, Academic Press, N. Y., 1964). The defect production in this case is much greater than that reported by Vavilov for A centers.

Since the Si-A center is known to be an effective recombination center, the previous results form the basis for the model of irradiation damage

and recovery in lithium-doped quartz-crucible silicon solar cells. The behavior in cells may follow the following model:



The apparent consumption of two lithium donors per annealing A center may be misleading. The data admits to the possibility of other defects with more shallow lying energy levels. It is entirely possible that some lithium donors are consumed in the annealing of such defects.

#### B. Carrier Removal Studies in Cells, Quartz-Crucible

In the previous quarterly report work was reported on a study of a quartz-crucible solar cell, AF-4921. The concentration of lithium donors at the junction ( $V_a=0$ ) and the short circuit current were studied during irradiation and recovery at 100°C. This data is again shown in Figure 4. In general, the results are very similar to those of float zone cells, in that a large decrease of lithium concentration occurs simultaneously with a recovery of the degraded short circuit current. The point of interest is that during the irradiation of  $3 \times 10^{15} \text{ e/cm}^2$ , only  $2 \times 10^{13} \text{ carrier electrons/cm}^3$  are removed. This is an order of magnitude lower than that observed in float zone cells. Since the lithium lost during recovery is comparable in both float zone and quartz crucible silicon, one can assume that similar numbers of radiation induced recombination centers were present in both types of cells. Even if the damage centers are un-ionized, the small quantity of carriers removed during irradiation would not indicate a lithium loss adequate to allow a lithium atom in the structure of each damage center. This result tends to support the need for an entirely different damage center in the case of quartz-crucible cells.

A more extensive analysis of the above sample was recently completed. By use of capacitance measurements, the donor concentration was determined at depths up to 5 microns into the n-type region. This data is shown in Figure 5. It can be seen that the small "loss of donors" during irradiation is a general condition which extends deep into the n-type region. The change which occurs during the 500 hour recovery period appears to vary

greatly with distance into the cell. To permit a closer analysis of the data, it was converted into removal rates ( $dn/d\phi$ ) and plotted as a function of distance into the n-type region. The removal rates during irradiation and recovery are both shown in Figure 6 as a function of distance. It is readily apparent from this data that the low apparent removal rate ( $0.006 \text{ cm}^{-1}$ ) during irradiation extends deep into the n-type region. The removal rate during recovery rises very rapidly with distance. A different view of this data is shown in Figure 7 where two removal rates are plotted as functions of the lithium donor concentration at a point in the cell where the particular removal rate was determined. Two facts are apparent; the removal rate during irradiation is not a function of lithium concentration, and the removal rate during recovery is a very strong function of the lithium concentration.

The results of lithium-doped quartz-crucible cell irradiation can be explained with a model consistent with previously discussed Hall coefficient measurements. To explain the results in these cells, one needs to examine various parameters relating to various charge states in the cell. The Fermi level in the n-type region near the junction is 0.28 eV below the bottom of the conduction band. A further calculation indicates that the Fermi factor or fraction of ionization for Si-A centers is only 0.03. This means that if such defects were generated during irradiation, only 3% of the Si-A centers would be ionized. This ionized fraction would be the only portion detected by carrier removal measurements at room temperature. Assuming the above situation, the introduction rate of Si-A centers would actually be  $0.006/0.03$  or  $0.2 \text{ cm}^{-1}$ . This is the same value determined by Hall coefficient measurements, as discussed in the previous section. It is also interesting to note that the removal rate during recovery appears as if it may be approaching a maximum value near  $0.2 \text{ cm}^{-1}$ . Such behavior would indicate the reaction of one lithium donor with one Si-A center during the recovery process. There is insufficient evidence to confirm such a relationship at this time.

All evidence available appears to support the model discussed in the previous section. In such a case the Si-A center would act as the dominant recombination center after irradiation. Specifically, the facts which support this model are:

1. Carrier removal during irradiation is very low, indicating that lithium is not consumed in forming damage complexes.
2. Carrier removal during irradiation is consistent with formation of Si-A centers.
3. Carrier removal during irradiation is independent of distance from the junction and lithium concentration, as contrasted with behavior to be discussed for lithium-doped float-zone silicon solar cells.
4. Hall coefficient measurements specifically indicate formation, during irradiation, of a deep acceptor defect with energy level near 0.17 eV below the conduction band.
5. Hall coefficient measurements also indicate that the above defect concentration decreases during recovery treatment and the lithium donor concentration decreases simultaneously.

#### C. Carrier Removal Studies in Cells, Float-Zone

Up to this time the full potential of the capacitance measurement has not been utilized in the examination of irradiated solar cells. In this section the changes in carrier concentration during and after irradiation are analyzed for three lithium-doped, float-zone solar cells of widely varying lithium concentrations. The current-voltage plot for Cell C3-18 is shown for several stages of irradiation and recovery in Figure 8. In Figure 9 the donor concentration as a function of distance into the n-type region is shown for the same cell in the same stages of irradiation and recovery illustrated in Figure 8. It appears the donor removal during irradiation is a strong function of distance into the n-type region. In addition the amount of donors removed during recovery for 200 hours is much larger than that removed during irradiation. After 400 hours the lithium donor concentration deep in the cell has risen somewhat, apparently from diffusion of lithium into this region. The increase in lithium concentration is probably the cause of the slight redegradation in short circuit current which occurs between 200 and 400 hours after irradiation. The data relating to donor concentration changes is replotted in Figure 10 for various depths in the

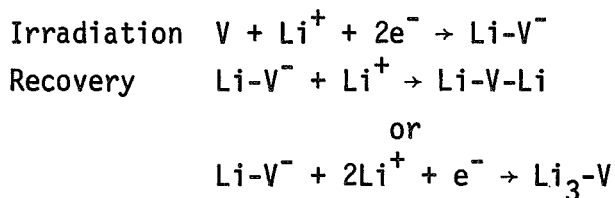
n-type region as a function of electron fluence. The data in Figure 10 indicates that the removal rate appears linear with electron fluence. The removal rate, however, increases rapidly with distance into the n-type region. The removal rate at the original edge of the space charge region ( $1.4\mu$ ) is only  $0.04\text{ cm}^{-1}$ . Measurements made with barrier width at  $3.7\mu$  indicate a removal rate of  $0.206\text{ cm}^{-1}$ . A five-fold increase in removal rate has occurred in a distance of only  $2.3\mu$  from the original unbiased space charge region.

Cell C3-18 is typical of a low lithium cell. The initial lithium concentration at the junction was  $3.8 \times 10^{14}\text{ atoms/cm}^3$ . A similar study will now be discussed for a cell with a somewhat higher lithium concentration. The solar cell current-voltage characteristic of Cell AF 14-4903 is shown in Figure 11 for several stages of irradiation and recovery. Figure 12 presents the results of the capacitance analysis during stages shown in Figure 11. In general, the donor concentration changes in Cell AF 14-4903 are very similar to those discussed for Cell C3-18. After 312 hours of recovery the donor concentration is approaching that of the original phosphorus concentration ( $2 \times 10^{14}\text{ atoms/cm}^3$ ) of the silicon. To further analyze the data in Figure 12, the donor concentrations for specific widths of the space charge region (distance into the n-type region) is replotted in Figure 13 as a function of electron fluence. In Cell AF 14-4903 the removal rates found during irradiation are somewhat higher than those found in Cell C3-18. A rapid increase in removal rate is also noted with increases in barrier width.

An additional cell (T4-10) with a much higher lithium concentration was studied in the same manner. The current-voltage relationships are shown for before and after irradiation and after recovery in Figure 14. The lithium concentrations as a function of barrier width for Cell T4-10 are shown in Figure 15. In this cell the lithium concentrations are large enough at all depths to allow recovery without making major changes in the lithium concentration. It can be noted that the lithium loss during irradiation is exceeded by that during recovery by 50 to 100%. This data is of importance in formulating a physical model for the process. The removal rates during the irradiation of Cell T4-10 at various distances into the n-type region are shown in Figure 16. Similar data is also shown

for Cells AF 14-4903 and C3-18. Figure 16 provides graphic sample of the extreme variation of removal rate (during irradiation) with depth that is possible within this type of solar cell. These variations may, in part, be responsible for the wide differences in removal rate reported by different investigators. The exact reason for this pattern of removal rate is not clear. The trend can be roughly described as a tendency for the removal rate to go to zero at the position of zero barrier width and rise rapidly from this value in some manner directly related to the lithium donor concentration. To further clarify this relationship the removal rate data was replotted versus the lithium concentration at the point in the cell at which the rate was determined. It is very obvious from the data in Figure 17 that certain lithium concentrations will not result in a specific removal rate. A particular point of interest regarding Figure 17 is that removal rate data for Cell AF 14-4903 and T4-10 do show near linear behavior in respect to lithium concentration. The fact that the individual curves are considerably displaced indicates the presence of some other strong factor in the determination of the removal rate. It is possible that distance from the space charge region edge and lithium concentration both act to determine the removal rate during irradiation of lithium-doped float-zone silicon cells. It is reasonable to expect the lithium concentration to affect the removal rate during irradiation. Simple mass action principles suggest that areas with higher concentrations of lithium donors should capture more displacement produced vacancies before annihilation than similar areas of lower lithium concentration. It is more difficult to postulate an independent effect which would cause the apparent defect production rate to be so low adjacent to the space charge region and increase so rapidly with distance from the barrier.

These results tend to support a previously preposed model of the damage and recovery processes. The model is as follows:



The data which supports this model is as follows:

1. Lithium is apparently consumed during the irradiation
2. Lithium is apparently consumed during the recovery
3. The lithium consumed during recovery is roughly equal to or greater than that consumed in irradiation.

## II. LITHIUM SOLAR CELL EVALUATION

In this phase of the program lithium-doped solar cells from the three manufacturers, Centralab, Heliotek, and Texas Instruments, have been irradiated with electrons and their recovery characteristics have been studied. Several different processing experiments were represented in these cells, including an oxygen layer adjacent to the junction, lithium diffused through both front and back surfaces, phosphorus  $n^+$  layer near the junction, and cells processed from whole slices. The groups evaluated, C8A through C8H, H8, T9, and T10, are listed, along with their material and processing variables, in Table I.

All of the cells received a radiation exposure of  $3 \times 10^{15}$  e/cm<sup>2</sup> at 1 MeV. Tungsten I-V characteristics and capacitance versus voltage measurements were then obtained as a function of time at either room temperature or 100°C. The general radiation damage and recovery characteristics of each group of cells are summarized in Table II. The recovered levels given in the table are the peak of the recovery curve and do not take into account any redegradation that may have occurred. The one-half recovery time is the time necessary for the short circuit current to reach a point midway between the damaged level and the peak recovery level. In general it can be observed that the higher lithium concentrations result in lower initial characteristics, higher recovered levels, and more rapid annealing rates while with lower lithium concentrations, higher initial levels and slower recovery rates exist.

In Table III, the peak recovery levels are compared graphically with each other and with the equivalent damage level for contemporary 10  $\Omega$ -cm n/p solar cells. The spread of the data and the half recovery time are also shown. It should be noted that most cell groups tested here are not

only inferior in recovered level to the best groups tested previously but are also no improvement over contemporary n/p cells.

#### A. Centralab Cells

In Centralab groups C8A through C8D the important feature is an oxygen-rich layer approximately 1 mil thick formed by diffusion in an oxidizing atmosphere prior to formation of the  $p^+$  layer. The hope was that this oxygen layer would prevent redegradation of the recovered level without affecting the bulk-dependent rapid recovery in float-zone and Lopex material. However, in both the float zone cells (C8A and C8B) and the Lopex cells (C8C and C8D) the oxygen layer slowed the recovery rates by more than two orders of magnitude (see Figs. 18 and 19) at room temperature. This is reasonable since the capacitance data in Table I indicate lithium concentrations of an order of magnitude less in the oxygen layer cells than in the non-oxygen layer cells for both materials.

To find out if recovered levels were stabilized it was necessary to accelerate the recovery process for half of the cells by annealing them at 100°C. No noticeable stability improvement was seen for the float-zone cells, but in the Lopex case much less (2% versus 25%) redegradation was observed in the oxygen layer cells as compared to the non-oxygen layer cells after 1000 hours.

Centralab groups C8E through C8H had lithium diffused through the  $p^+$  layer on the front of the cells as well as through the back. The reasons for this experiment are to prevent excess lithium concentrations and severe lithium gradients. The initial outputs of the float-zone cells (C8E and C8F) were so poor, about 30 ma. for C8E, that they were not included in the testing program. The crucible grown cells (C8G and C8H) had fairly good initial outputs, were irradiated, and were annealed at 100°C (Fig. 20). Lithium concentrations in the front-back diffused cells were 3 to 10 times higher than in the back-only cells and, as expected, they annealed faster. However, the front-back diffused cells did not recover as far as expected with peak short circuit currents of only 30 ma. compared to 33 and 38 for the back-only cells.

### B. Heliotek Cells

The one Heliotek solar cell group (H8) which was included in this evaluation had a phosphorus  $n^+$  layer diffused near the junction prior to the boron  $p^+$  diffusion. Except for this additional phosphorus layer, these cells were identical to the H4 group tested last year. The H8 cells have recovered a few milliamps farther (37 versus 33) than the H4 cells, but at a factor of four more slowly (Fig. 21). The H7 cells tested last year and several other Heliotek groups are superior in recovered level with the best between 40 and 45 ma. and recovery rates similar to those for the H8 cells (Table III).

### C. Texas Instruments Cells

The Texas Instruments solar cell groups (T9 and T10) were processed from whole slices to eliminate potential edge effects due to non-uniform lithium concentrations. In addition, the lithium diffusion was designed to produce half the lithium concentration of Texas Instruments standard lithium cells in the T9 group and twice the standard concentration in the T10 group. The capacitance measurements confirm this plan, indicating a factor of four in lithium concentration between the two groups. Recovered levels for both groups (Figs. 22 and 23) are disappointing, however, as neither cell group reached 35 ma. while last year's T6 group reached 40 ma. As expected, the annealing rate of the T10 group is far faster than that of the T9 cells, but this rapid recovery is associated with a significant redegradation, about 35% after 700 hours. It is concluded, as in last year's final report, that the reducing of edge effects does not improve recovery performance.

### D. Summary

The results of the lithium solar cell evaluation program thus far are mostly negative in that none of the processing parameters represented in these cell groups has improved their recovery characteristics appreciably beyond the standard n/p damage level or produced cells as good as those tested in last year's program. The oxygen diffused specimens support previous conclusions in that the presence of oxygen slows the lithium diffusion with corresponding decreases in recovery rate and redegradation rate and no strong effect on maximum recovered level.

### III. PROGRESS IN THE NEXT REPORT PERIOD

During the next report period more Hall coefficient work is planned to confirm the charge state of the Li-V defect believed to be formed during irradiation of lithium-doped float-zone silicon. In addition, work will be done to study the effect of lithium in the irradiation of p-type silicon. Also, the lithium-doped solar cell evaluation program will continue.

### IV. NEW TECHNOLOGY

No new technology was developed in this report period.

Cell Group	<u>Base Material</u>		<u>Lithium Introduction</u>		
	Material Type	Dopant	Resistivity $\Omega$ -cm	Diffusion Schedule $^{\circ}\text{C}/\text{Min}/\text{Min}$	Li Concentration at Junction $\text{cm}^{-3}$
C8A	F.Z.	P	100	400/120	$3 \times 10^{14}$ Oxygen Layer
C8B	F.Z.	P	100	400/120	$4 \times 10^{15}$ Without Oxygen Layer
C8C	Lopex		90	400/120	$6 \times 10^{14}$ Oxygen Layer
C8D	Lopex		90	400/120	$4 \times 10^{15}$ Without Oxygen Layer
C8E	F.Z.	P	100	400/10	$> 1 \times 10^{16}$ Li Diffused Front and Back
C8F	F.Z.	P	100	400/120	$4 \times 10^{15}$ Li Diffused Back Only
C8G	Cruc.	As	30	400/10	$1 \times 10^{15}$ Li Diffused Front and Back
C8H	Cruc.	As	30	400/120	$< 10^{14}$ & $3 \times 10^{14}$ Li Diffused Back Only
H8	F.Z.	P	100	425/90/60	$6 \times 10^{14}$ Phosphorus Layer
T9	Lopex	P	>50	325/480	$9 \times 10^{14}$ Processed from Whole Slices
T10	Lopex	P	>50	400/135	$4 \times 10^{15}$ Processed from Whole Slices

TABLE I. Lithium Solar Cell Manufacturing Parameters

CELL GROUP	$N_{Li}$ cm <sup>-3</sup>	Annealing Temp. °C	Initial Level I <sub>SC</sub> , ma.	Damaged Level I <sub>SC</sub> , ma.	Recovered Level I <sub>SC</sub> , ma.	Time (hrs.) to 1/2 Recovery Point
C8A	$2 \times 10^{14}$	25	50	21	Not Yet Peaked	
	$4 \times 10^{14}$	100	47	18	36	< 1
C8B	$4 \times 10^{15}$	25	42	16	33	4
C8C	$5 \times 10^{14}$	25	51	20	Not Yet Peaked	
	$7 \times 10^{14}$	100	50	18	35	< 3
C8D	$4 \times 10^{15}$	25	50	18	33	1.2
C8G	$1 \times 10^{15}$	100	52	16	30	< 3
C8H	$4 \times 10^{14}$ & $3 \times 10^{14}$	100	60 & 48	25 & 17	38 & 33	7 & .5
H8	$6 \times 10^{14}$	25	37	22	36	12
T9	$9 \times 10^{14}$	25	53	15	33	20
T10	$4 \times 10^{15}$	25	47	18	30	< 1

TABLE II. Lithium Solar Cell Recovery Characteristics After  $3 \times 10^{15}$  e/cm<sup>2</sup>, 1 MeV

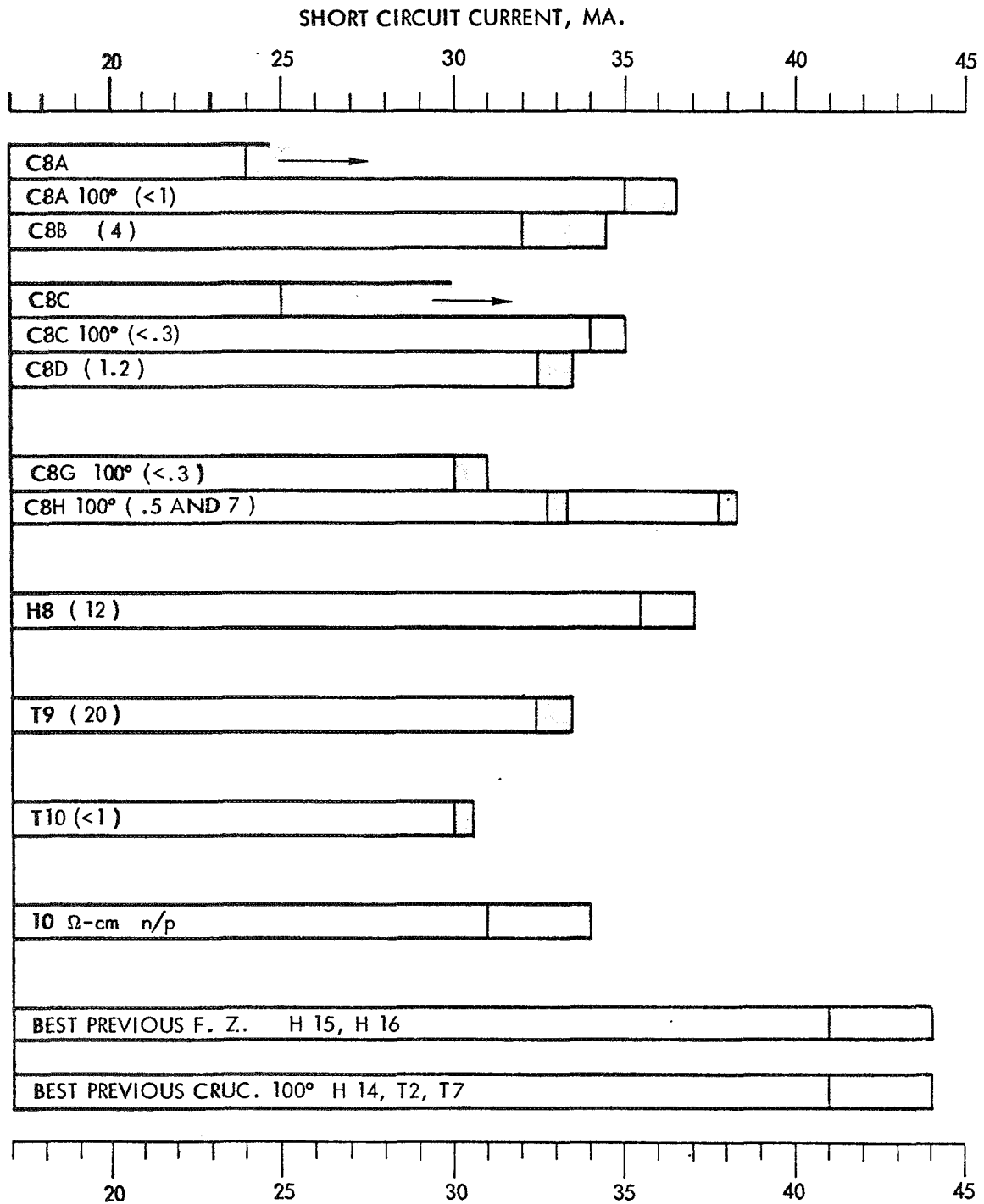


TABLE III. RECOVERED LEVEL AND HALF RECOVERY TIME (Hours)

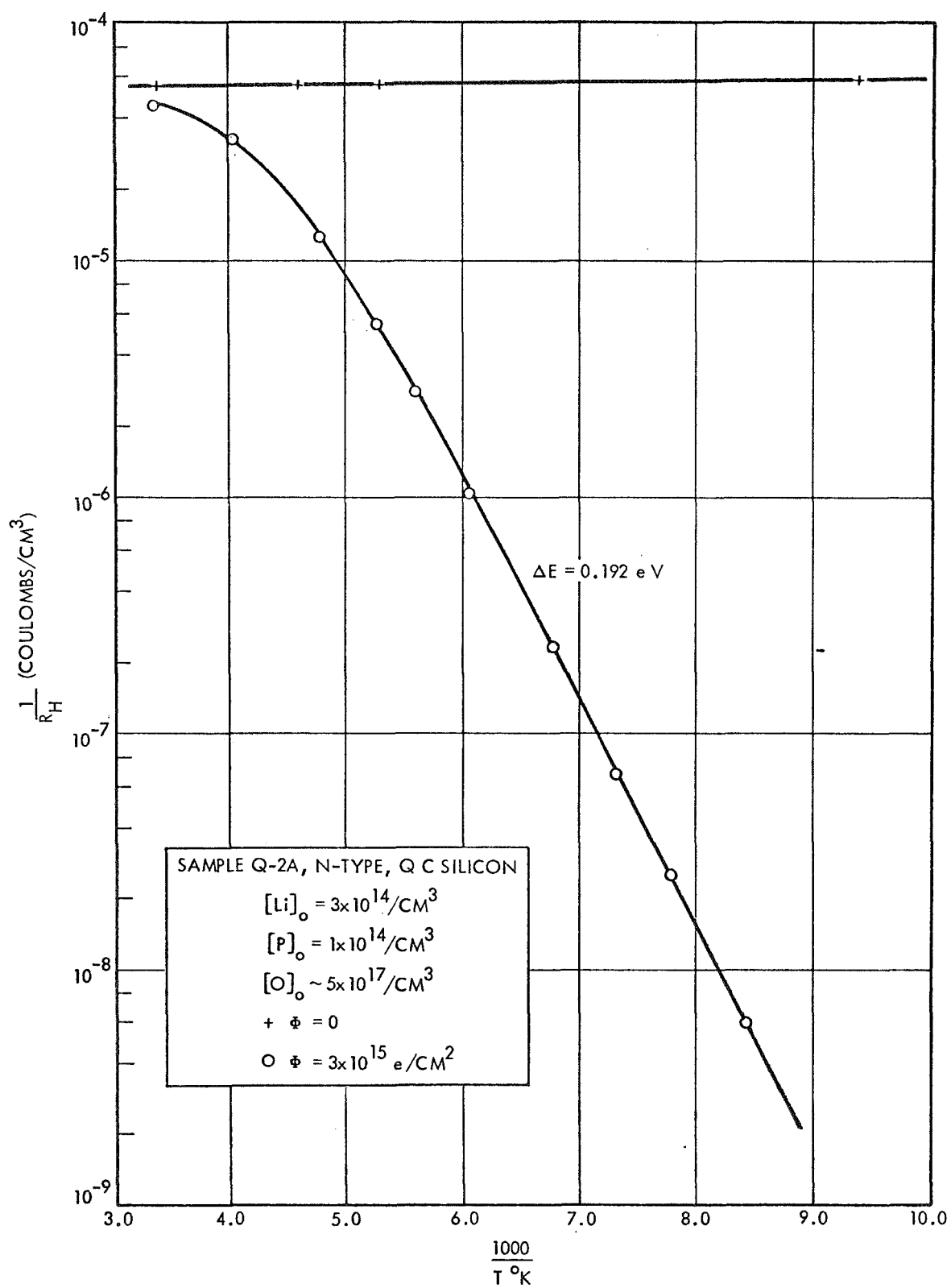


FIG. 1 HALL COEFFICIENT VS. TEMPERATURE, IRRADIATED LITHIUM-DOPED QUARTZ-CRUCIBLE SILICON

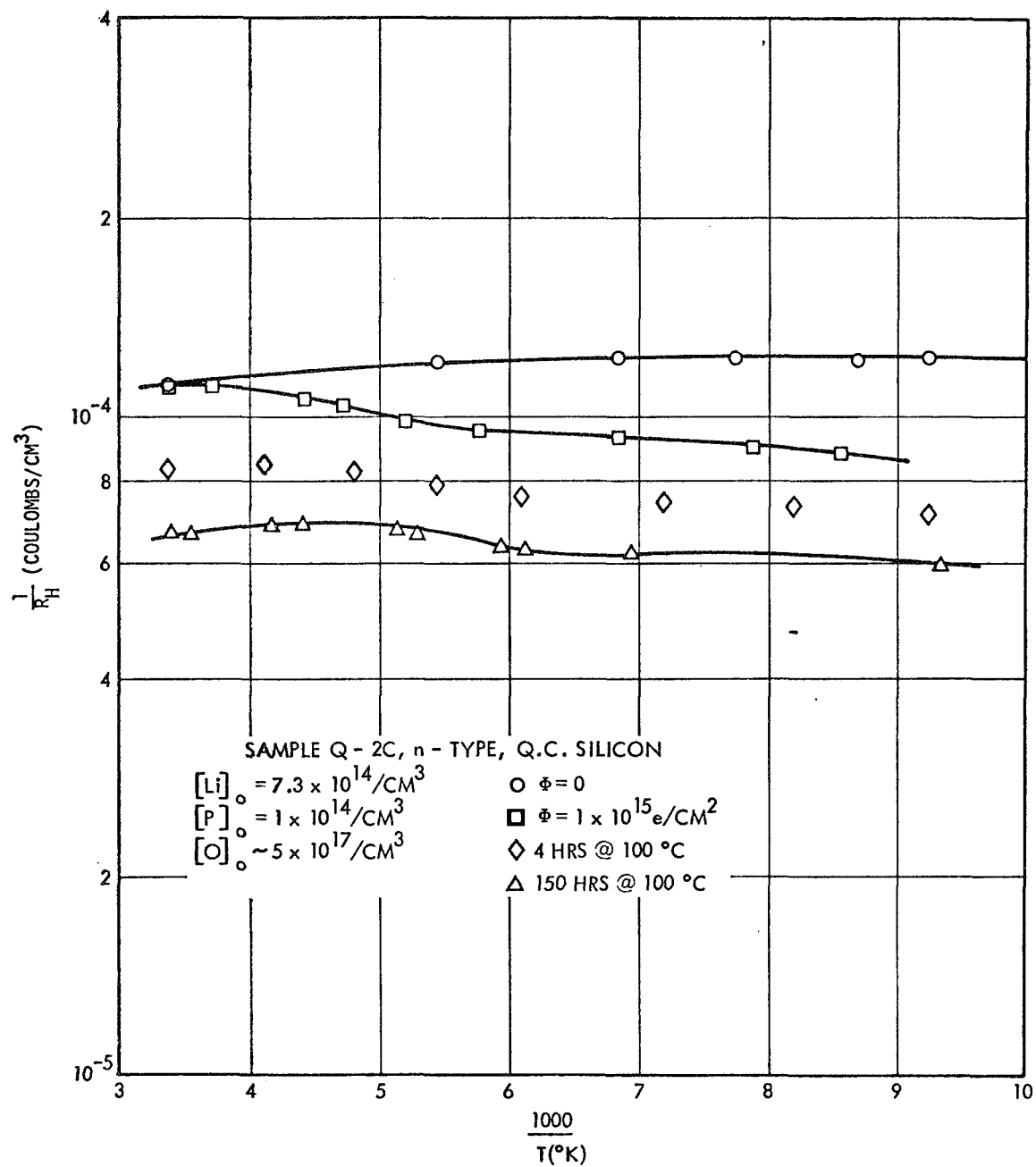


FIG. 2 HALL COEFFICIENT VS. TEMPERATURE, IRRADIATED LITHIUM-DOPED QUARTZ-CRUCIBLE SILICON

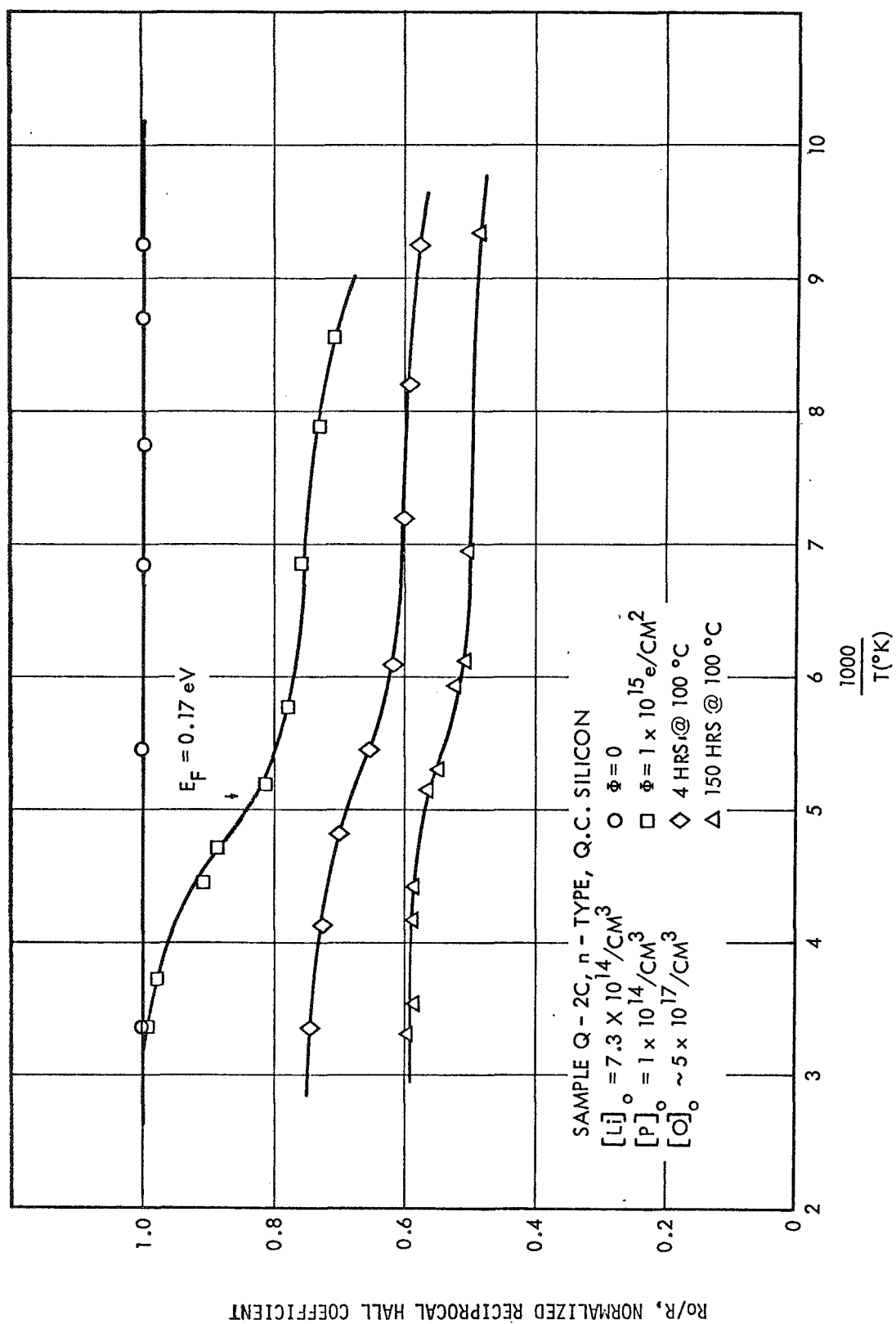


FIG. 3 NORMALIZED HALL COEFFICIENT VS. TEMPERATURE, IRRADIATED LITHIUM-DOPED QUARTZ-CRUCIBLE SILICON

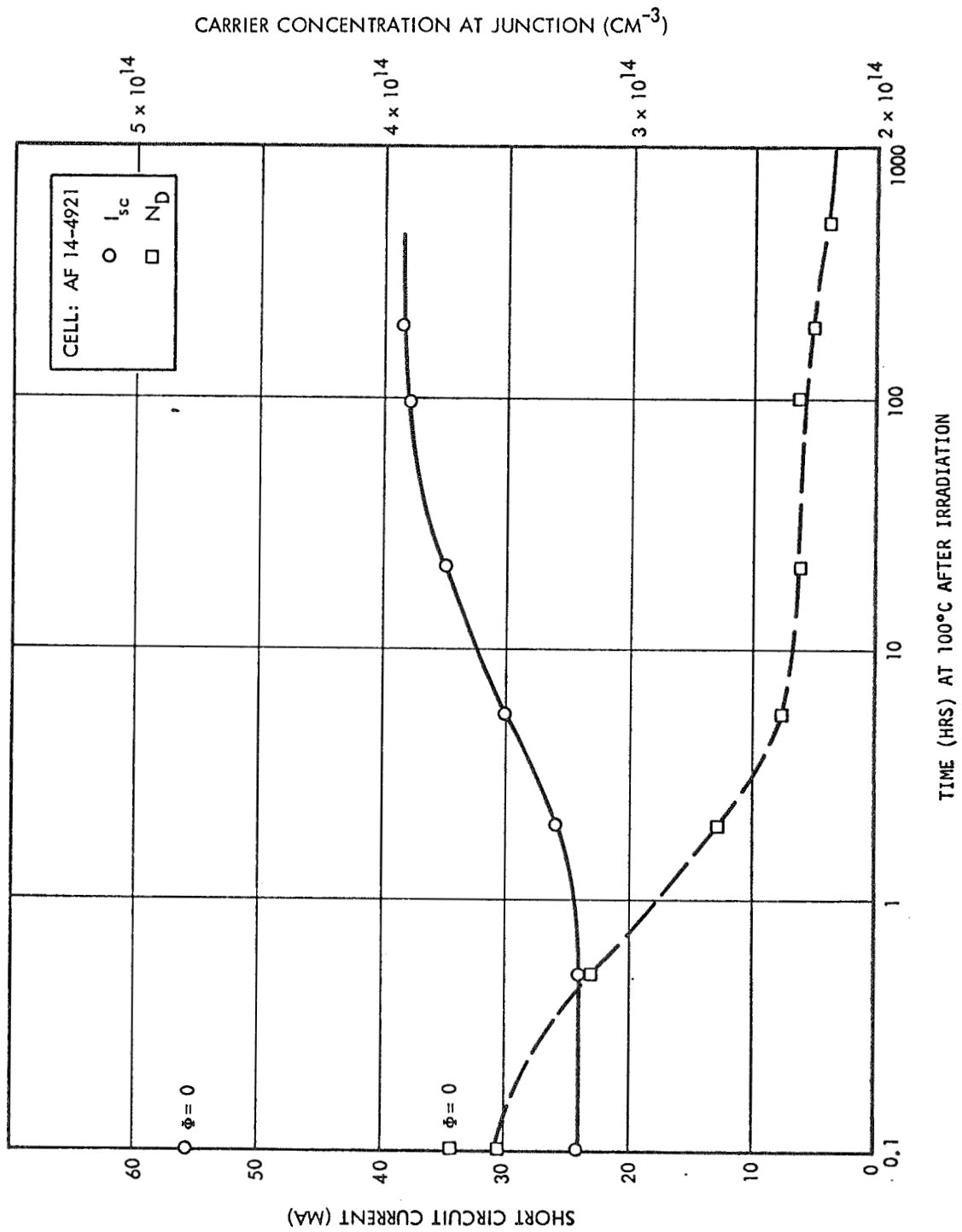


FIG. 4 RECOVERY OF LITHIUM-DOPED QUARTZ-CRUCIBLE CELL

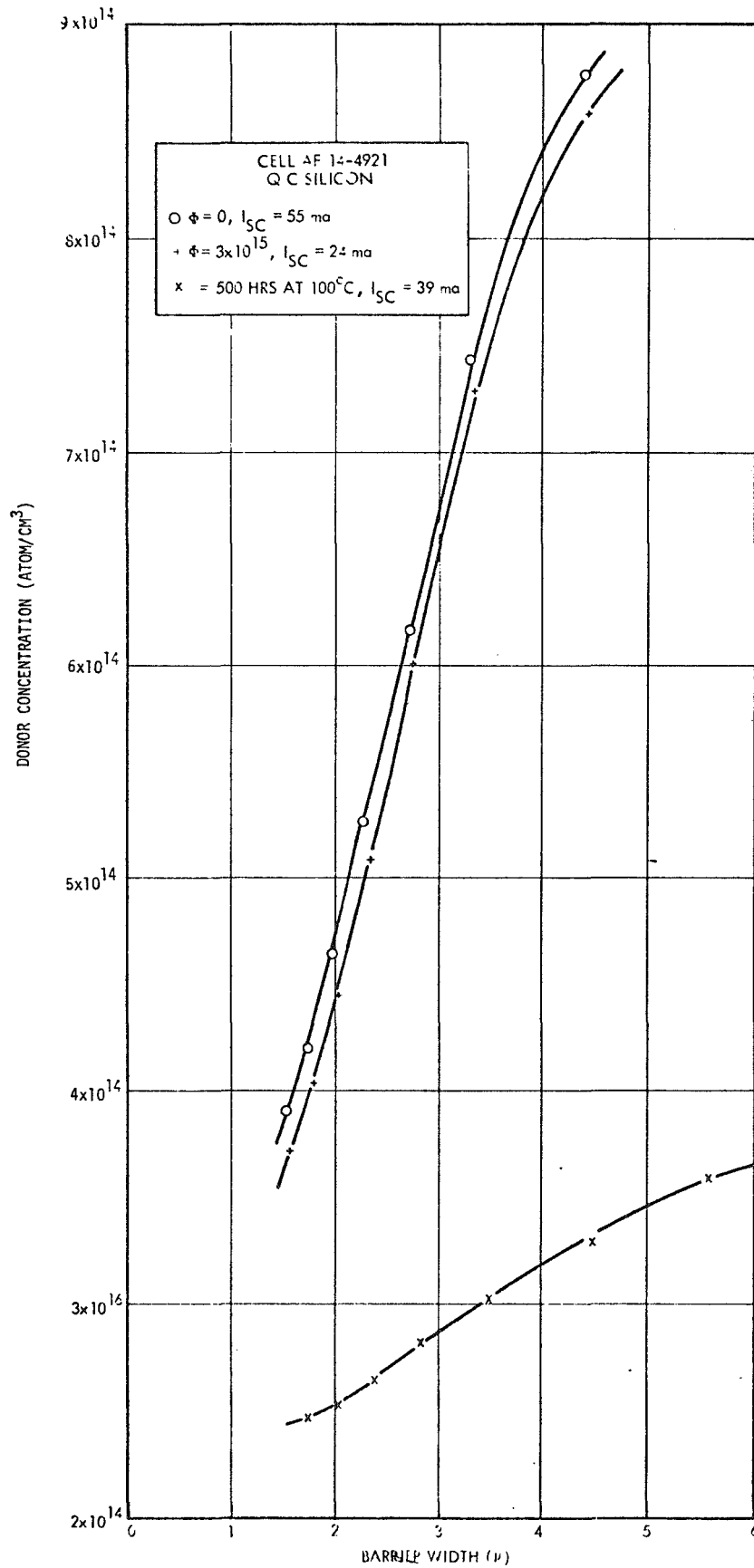


FIG. 5 DONOR CONCENTRATION VS. BARRIER WIDTH, CELL AF 14-4921

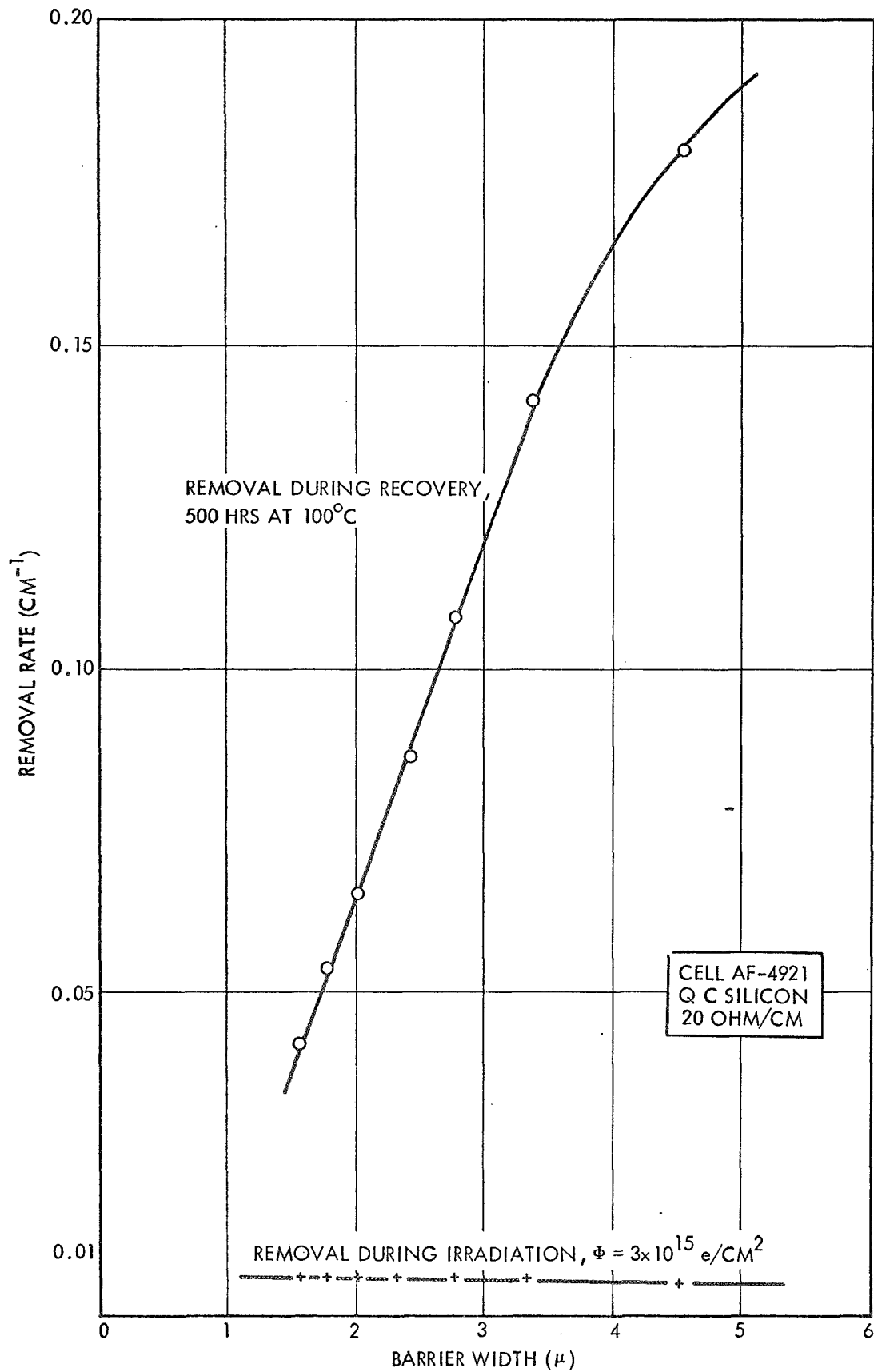


FIG. 6 REMOVAL RATE VS. BARRIER WIDTH, CELL AF 14-4921

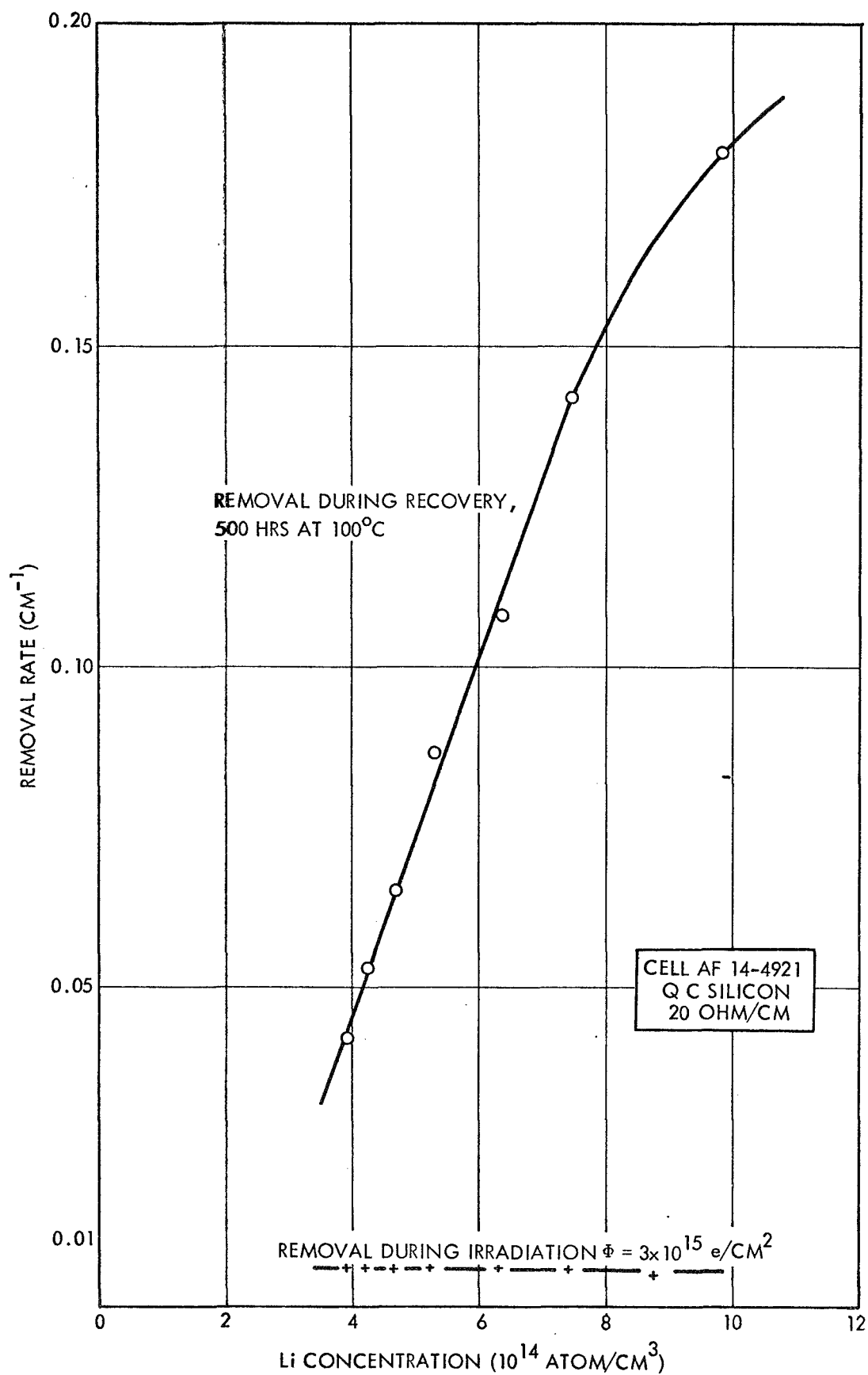


FIG. 7 REMOVAL RATE VS. LITHIUM CONCENTRATION, CELL AF 14-4921

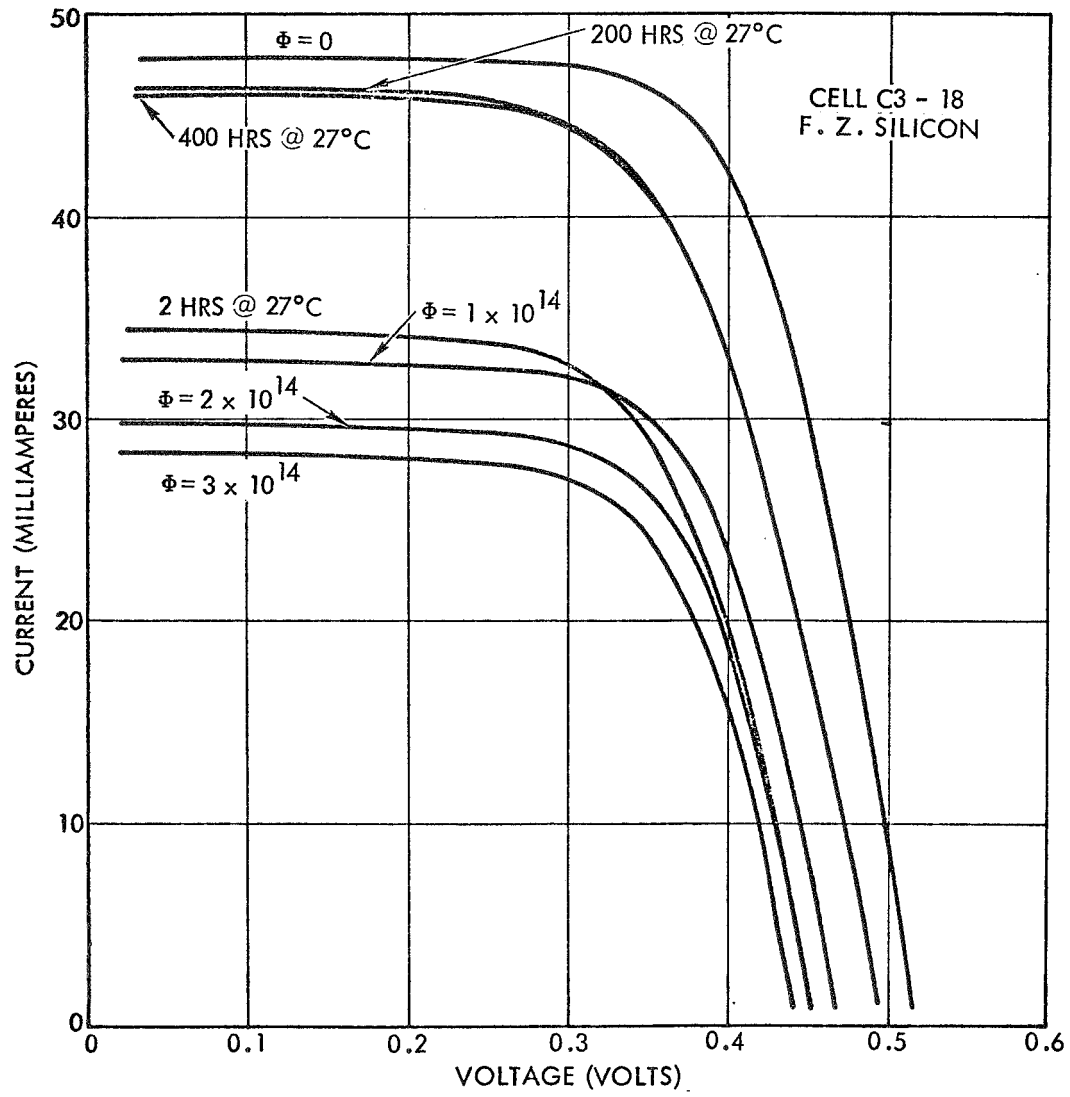


FIG. 8 SOLAR CELL CHARACTERISTICS, CELL C3-18

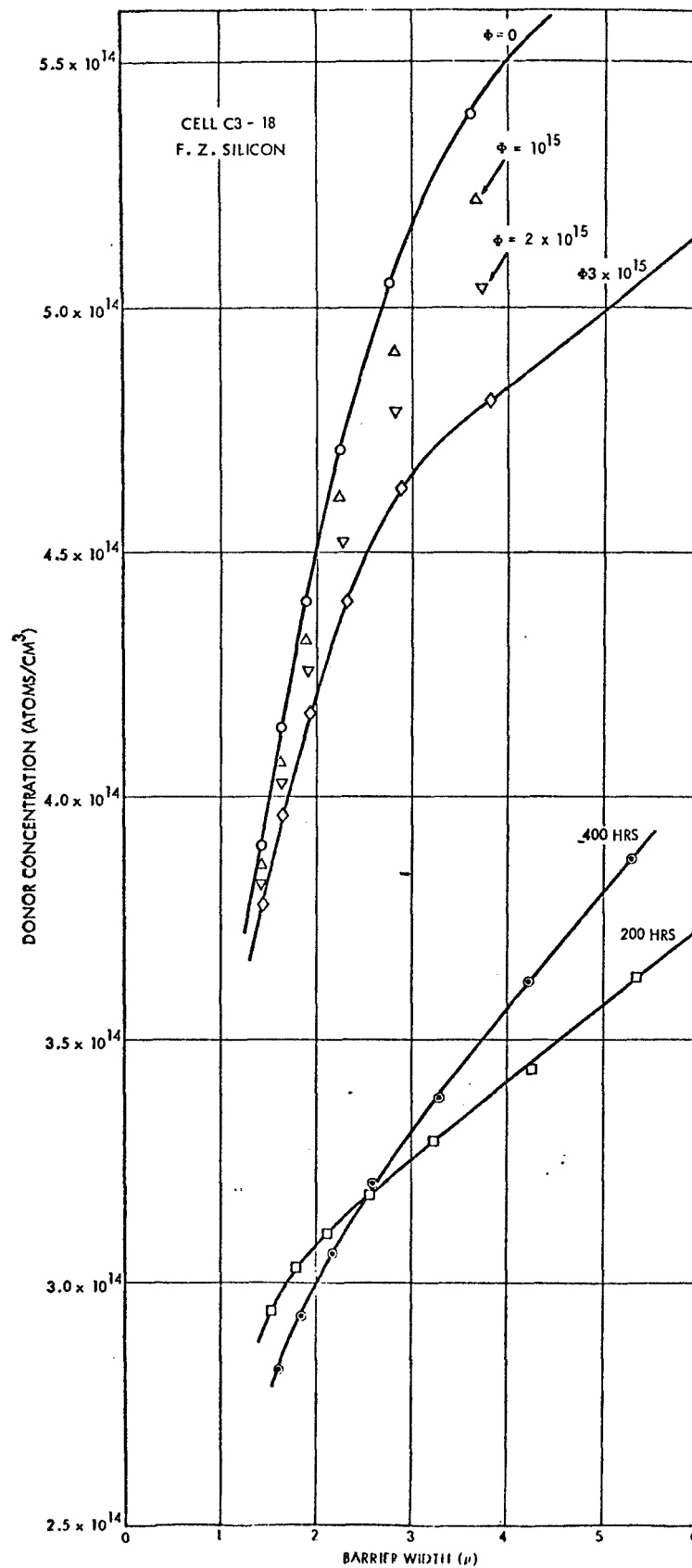


FIG. 9 DONOR CONCENTRATION VS. BARRIER, CELL C3-18

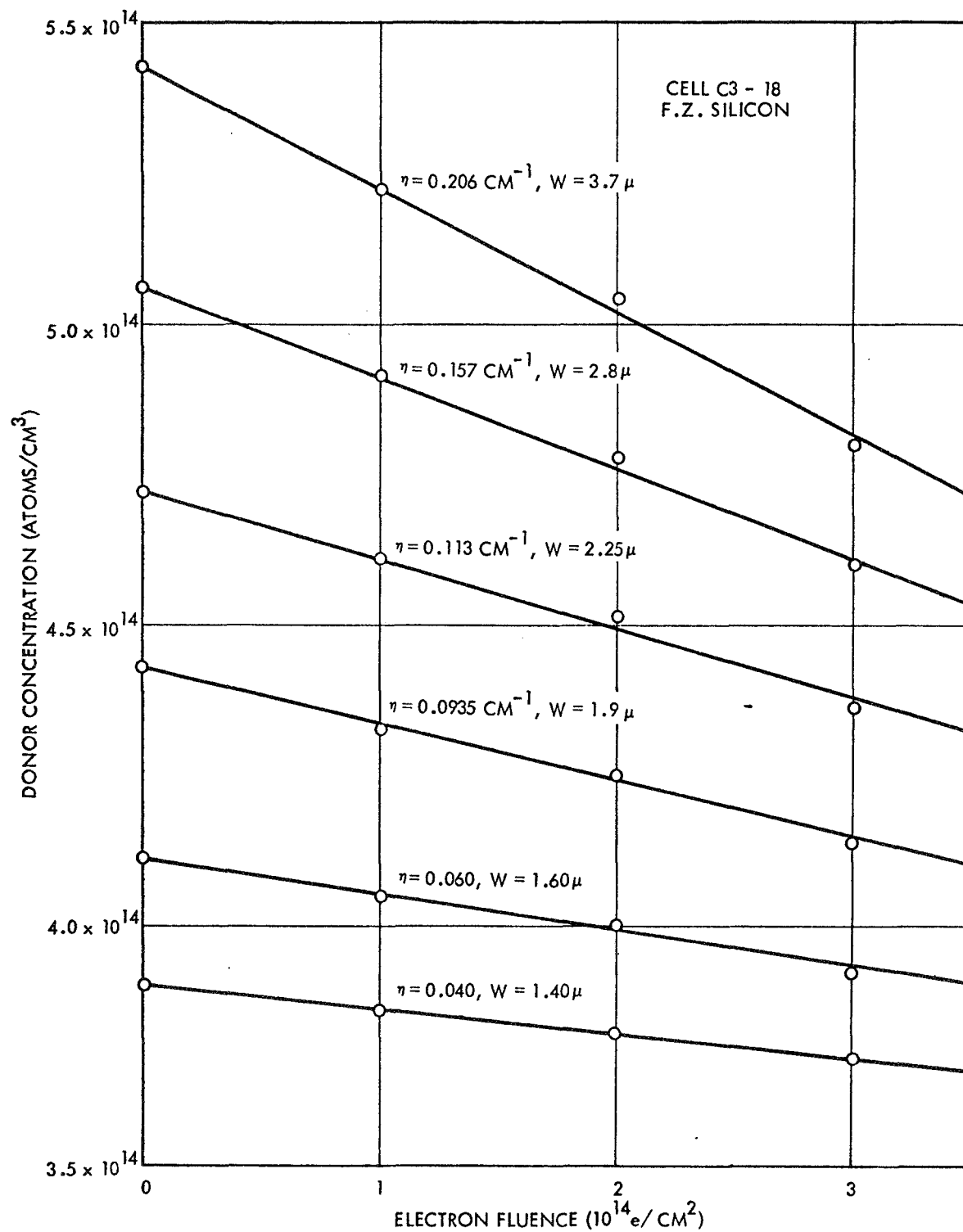


FIG. 10 DONOR CONCENTRATION VS. FLUENCE, CELL C3-18

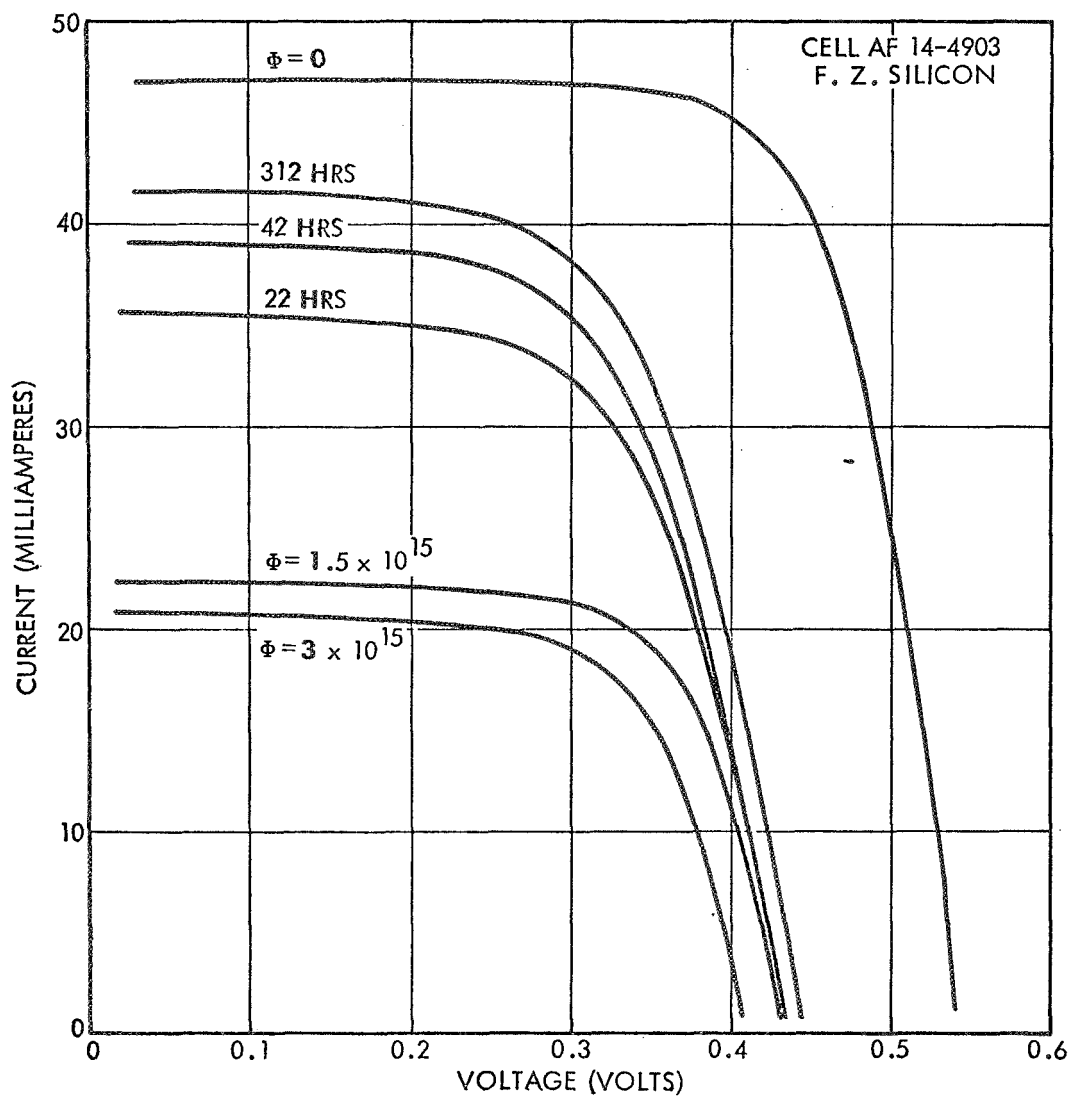


FIG. 11 SOLAR CELL CHARACTERISTICS, CELL AF 14-4903

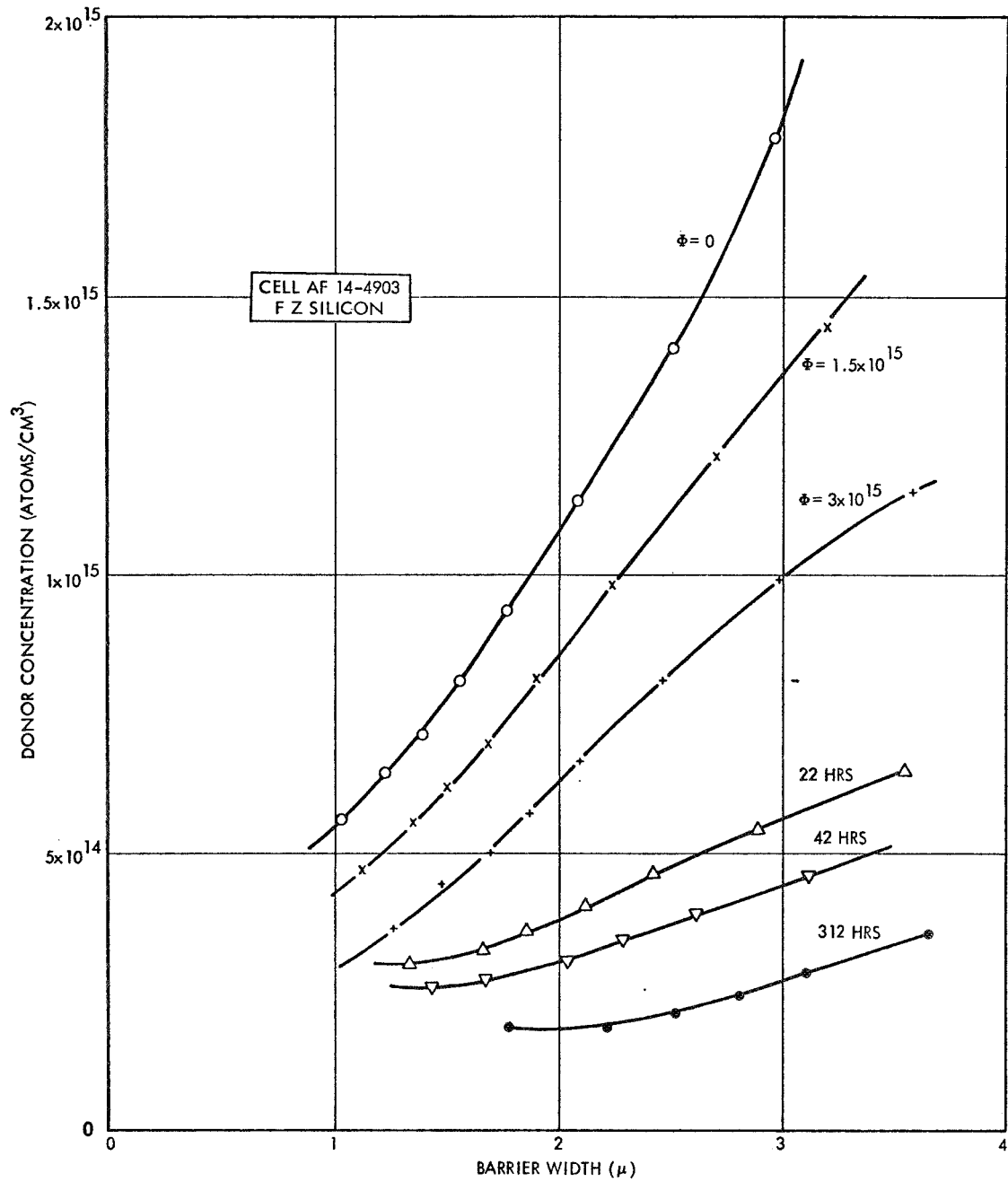


FIG. 12 DONOR CONCENTRATION VS. BARRIER WIDTH, CELL AF 14-4903

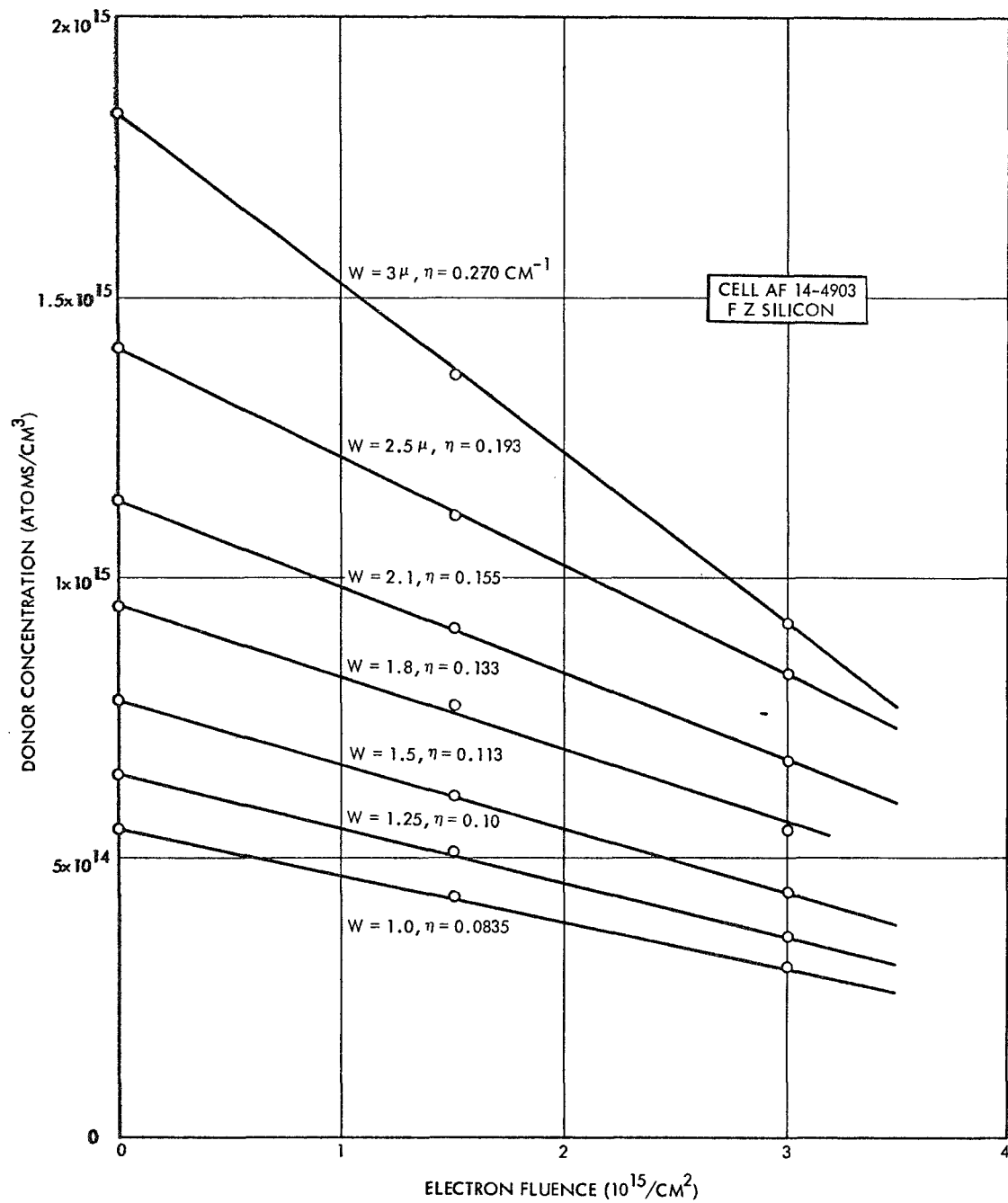


FIG. 13 DONOR CONCENTRATION VS. FLUENCE, CELL AF 14-4903

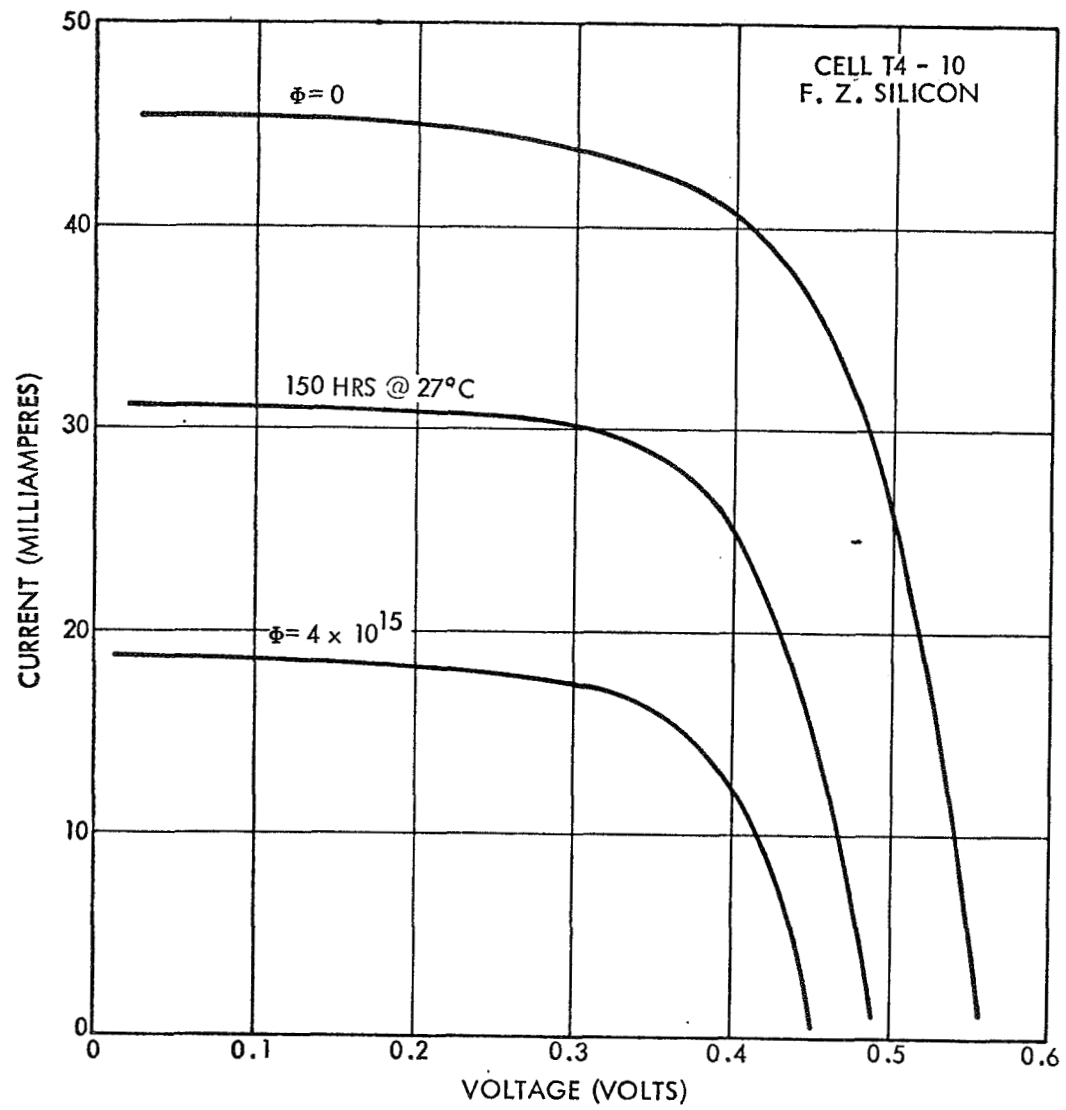


FIG. 14 SOLAR CELL CHARACTERISTICS, CELL T4-10

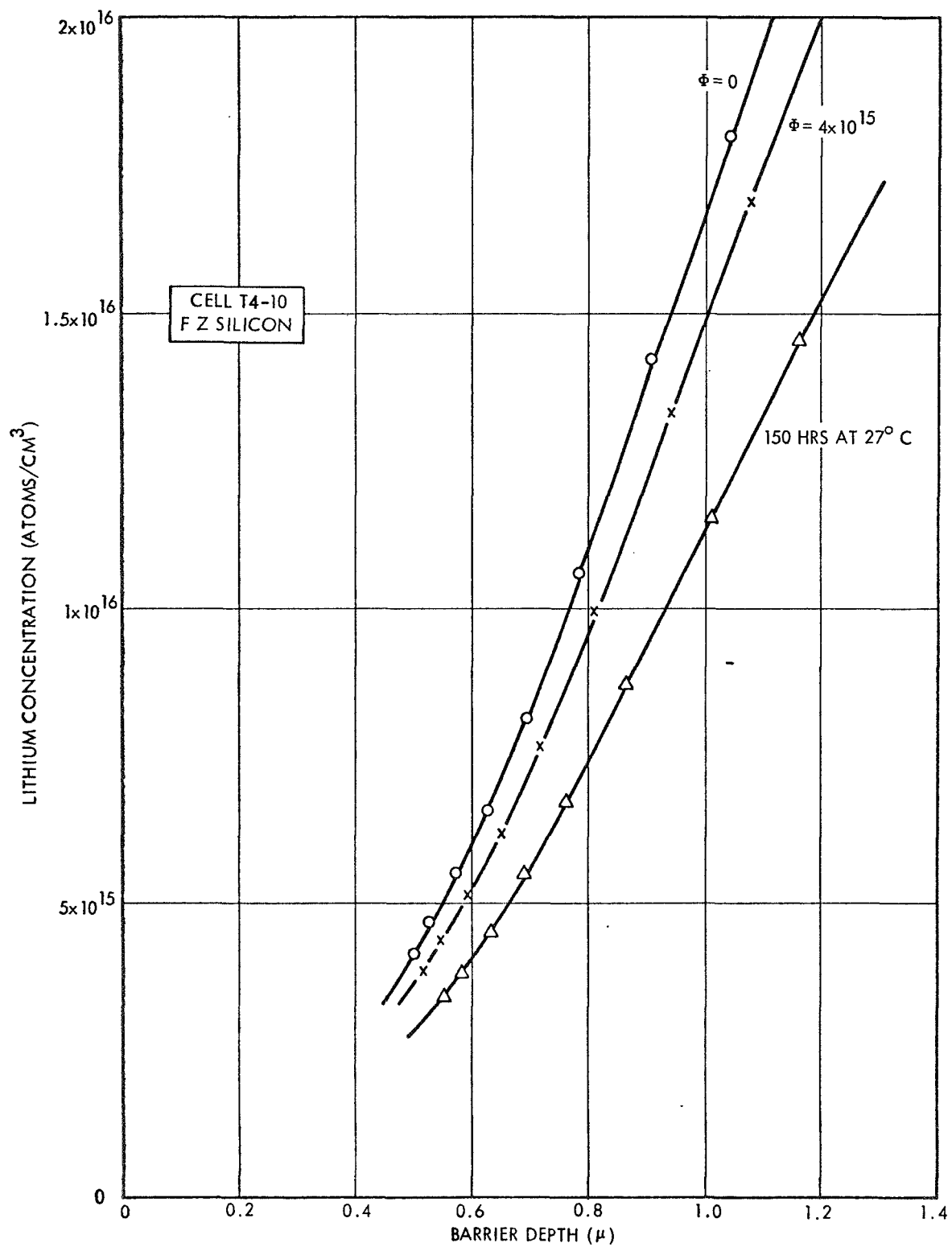


FIG. 15 DONOR CONCENTRATION VS. BARRIER WIDTH, CELL T4-10

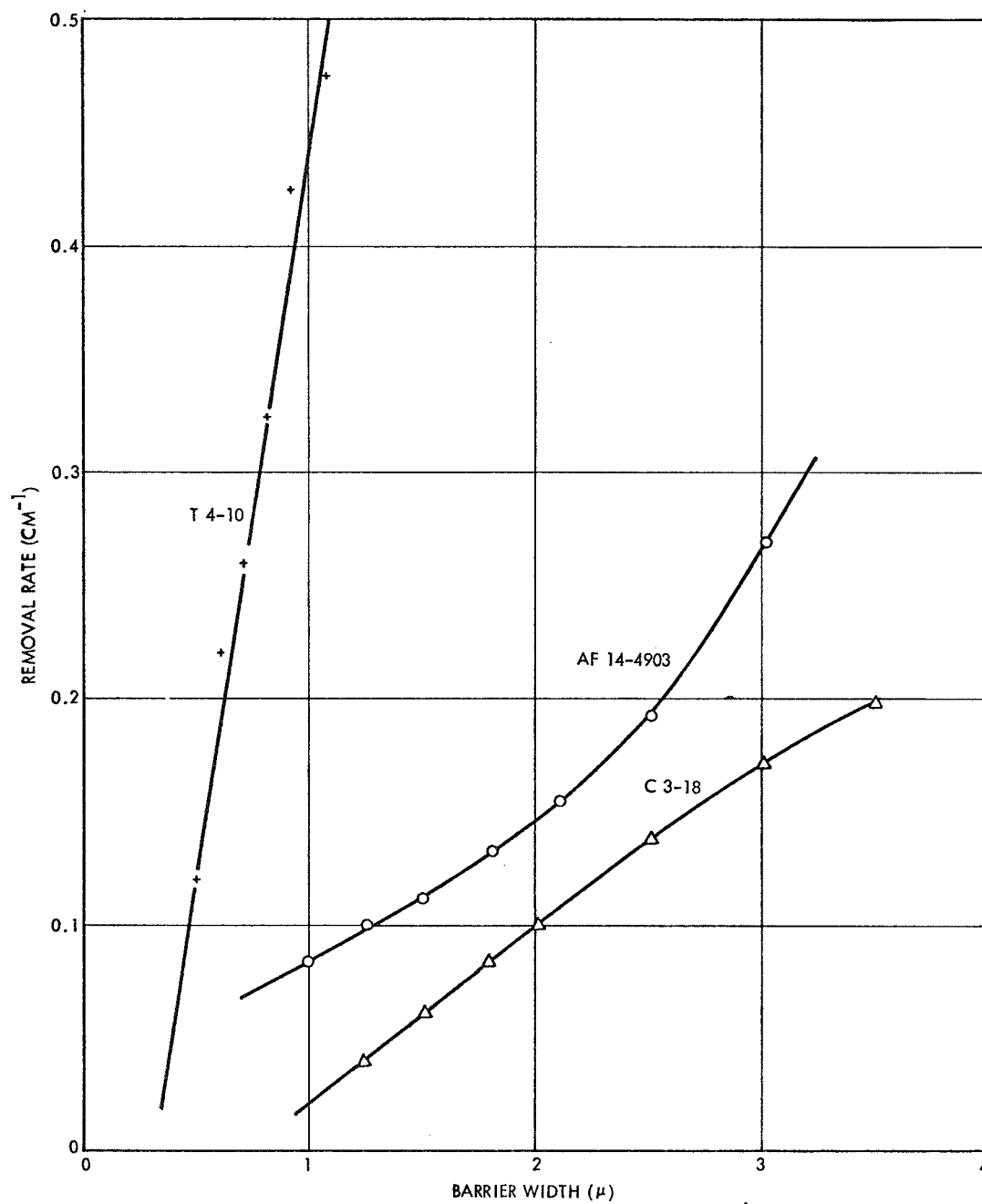


FIG. 16 REMOVAL RATE VS. LITHIUM CONCENTRATION,  
FLOAT-ZONE CELLS

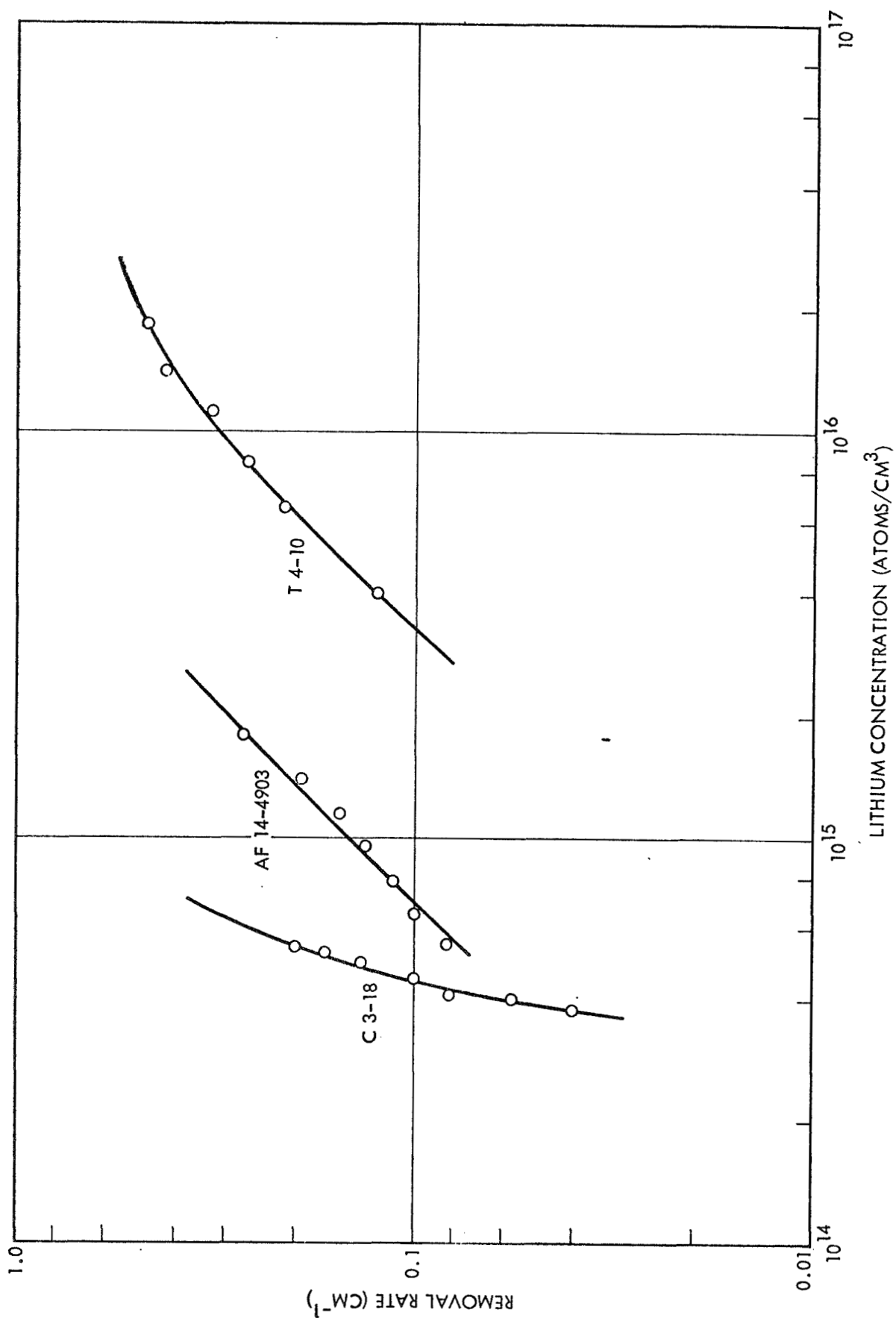


FIG. 17 REMOVAL RATE VS. BARRIER WIDTH, FLOAT-ZONE CELLS

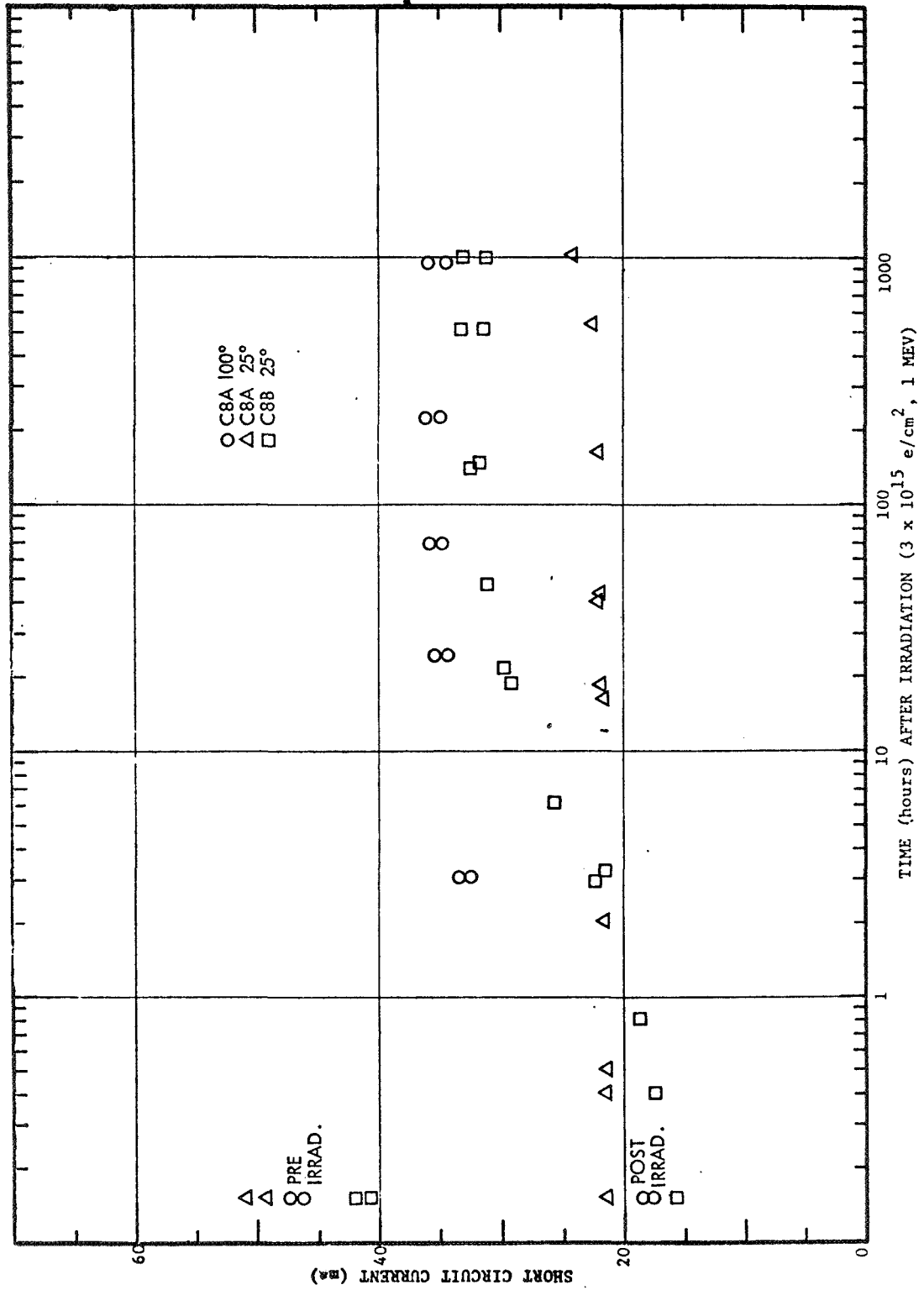


FIG. 18 RECOVERY OF GROUPS C8A AND C8B LITHIUM SOLAR CELLS

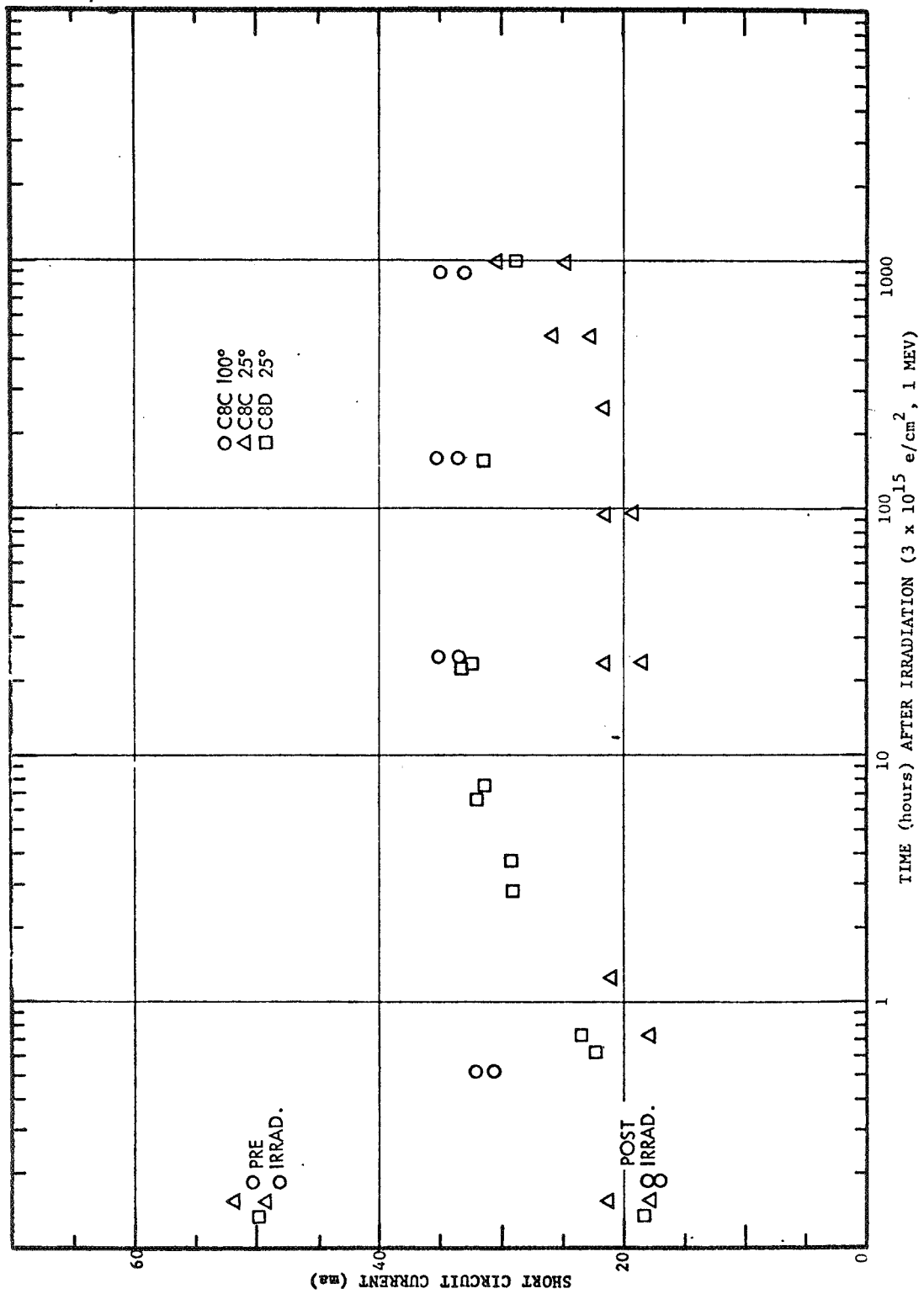


FIG. 19 RECOVERY OF GROUPS C8C AND C8D LITHIUM SOLAR CELLS

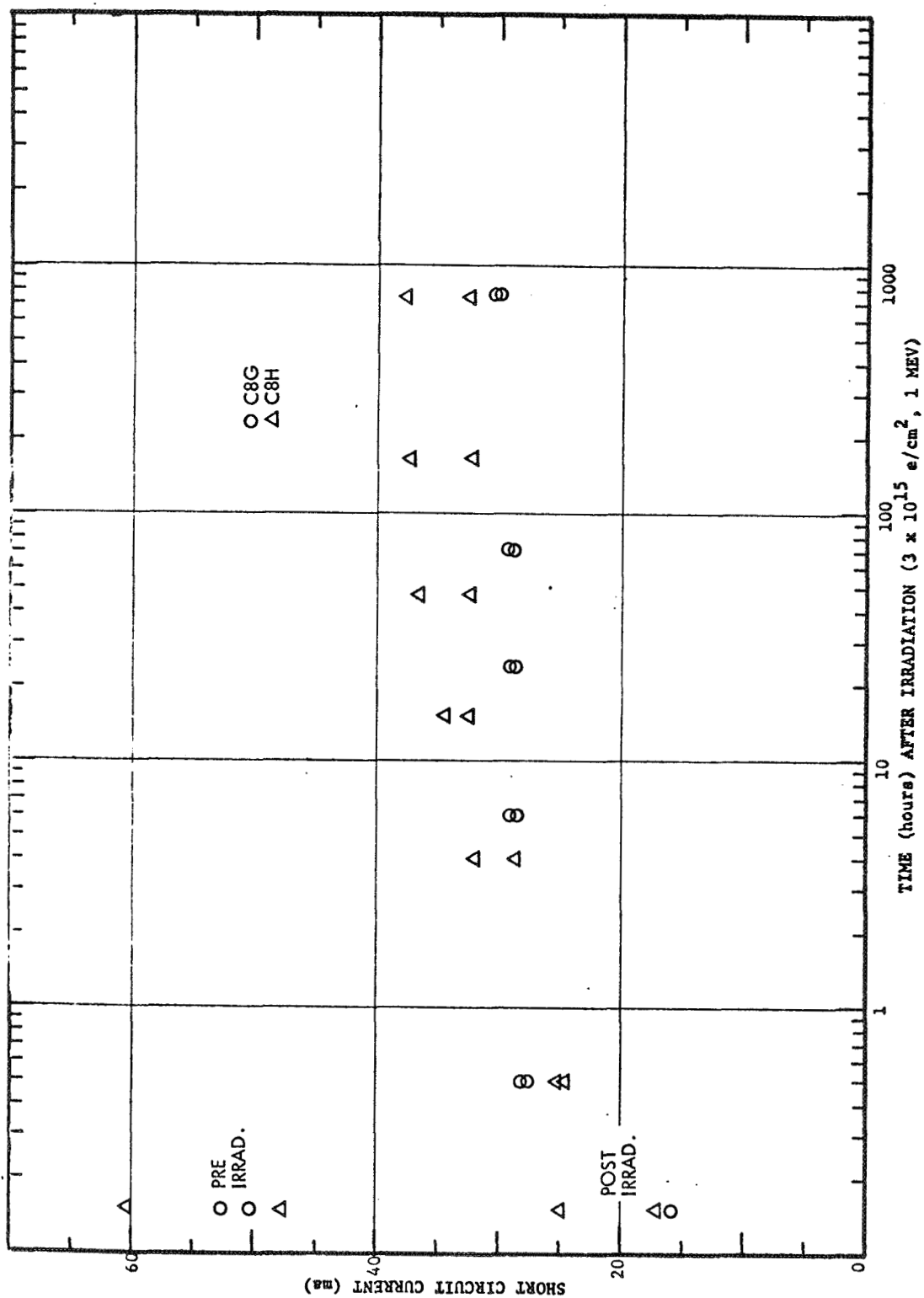


FIG. 20 RECOVERY OF GROUPS C8G AND C8H LITHIUM SOLAR CELLS

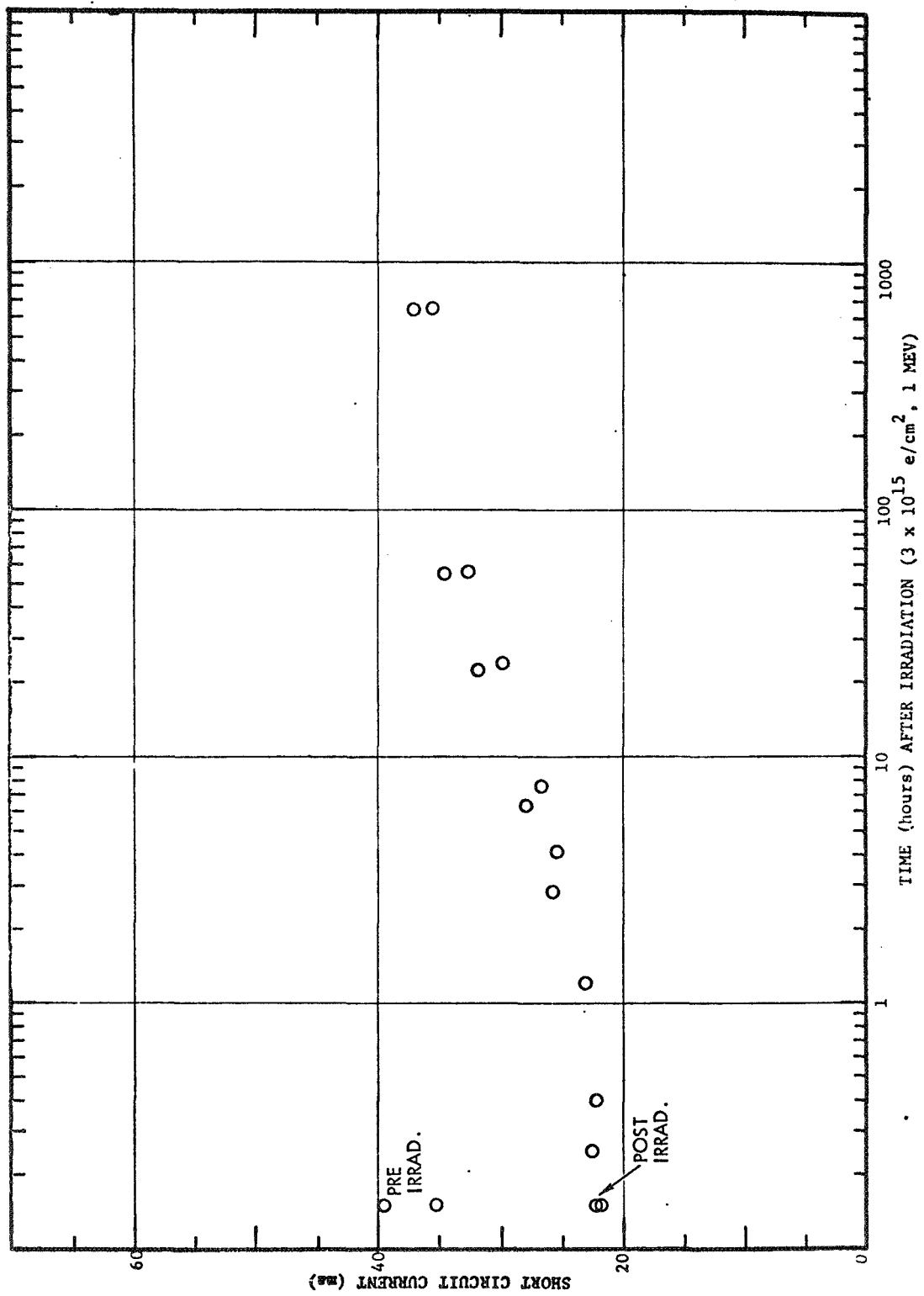


FIG. 21 RECOVERY OF GROUP H8 LITHIUM SOLAR CELLS

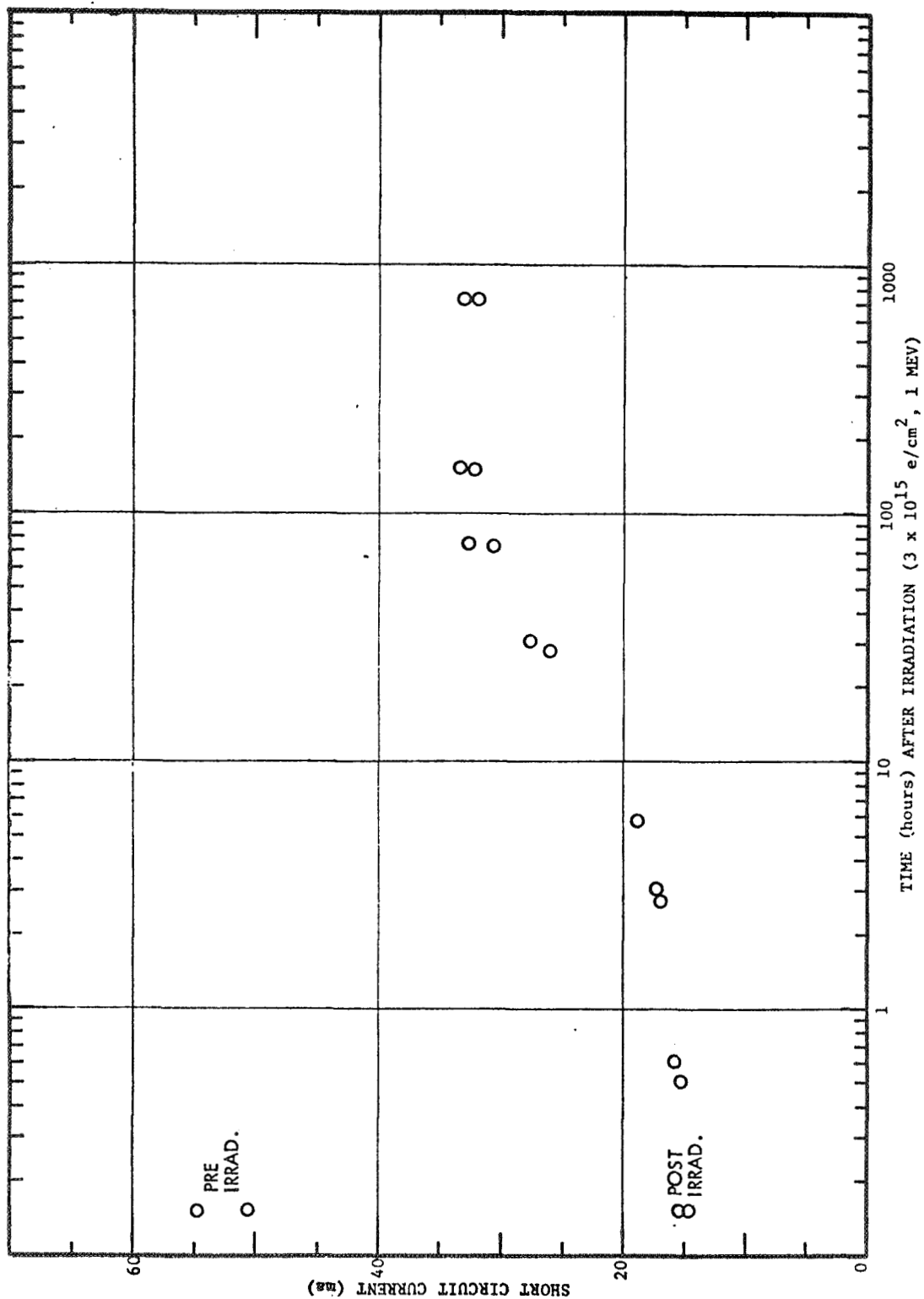


FIG. 22 RECOVERY OF GROUP T9 LITHIUM SOLAR CELLS

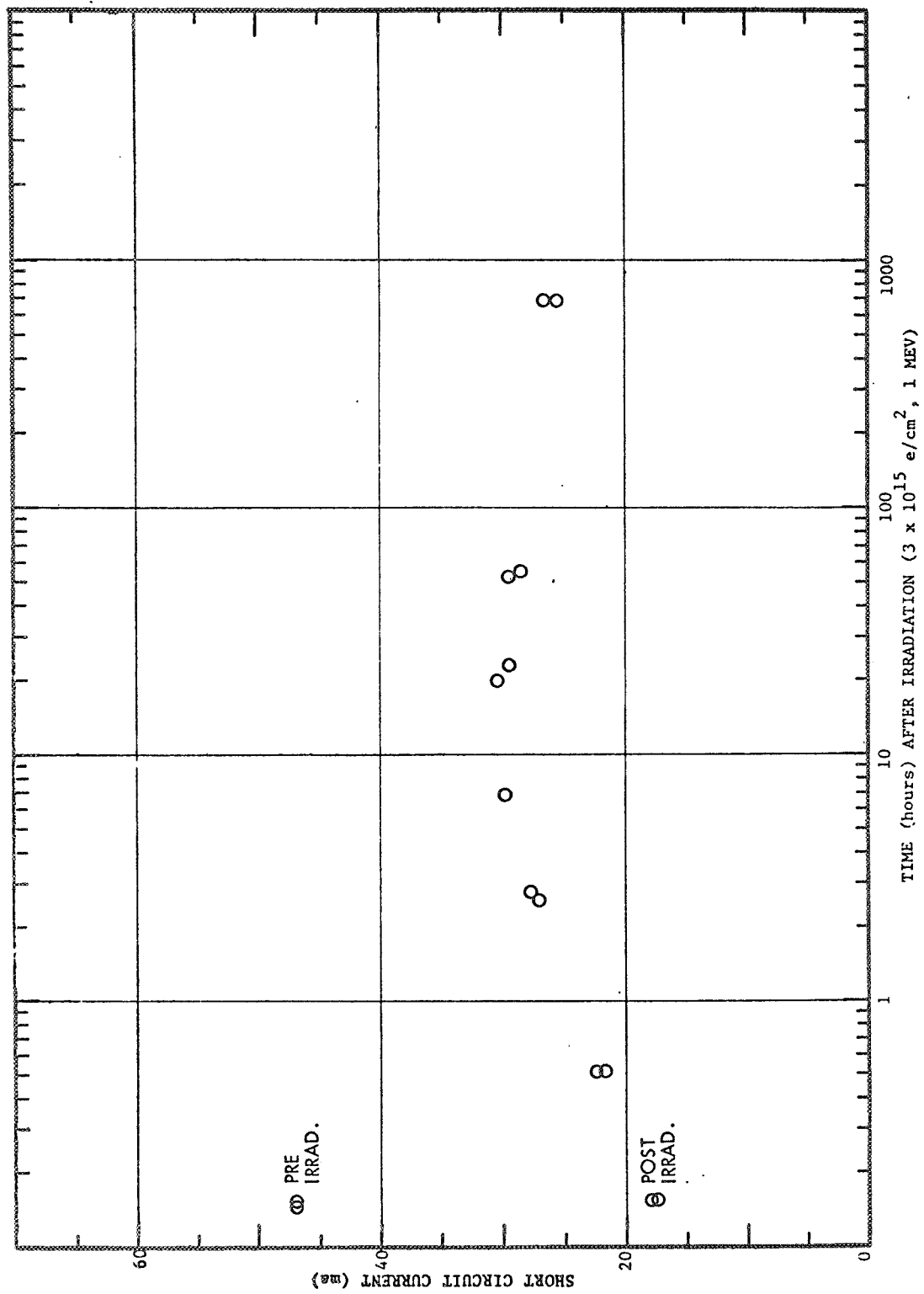


FIG. 23 RECOVERY OF GROUP T10 LITHIUM SOLAR CELLS